ERASMUS UNIVERSITY ROTTERDAM

ERASMUS SCHOOL OF ECONOMICS

Simulating Haemoglobin Concentrations for MISCAN-Colon Using Black-box Machine Learning as a Step Towards Personalised Colorectal Cancer Screening[1]

Author

Yoëlle Kilsdonk (513530)

Supervisors

E. P. O'Neill (EUR)

dr. I. Lansdorp-Vogelaar (EMC)

R. van den Puttelaar (EMC)

D. van den Berg (EMC)

Second assessor

dr. O, Vicil (EUR)

November 11, 2022

[1]The views stated in this thesis are those of the author and not necessarily those of the supervisors, second assessor, Erasmus School of Economics, Erasmus University Rotterdam or Erasmus Medical Centre.

Abstract

Keywords— MISCAN, Machine Learning

Table of contents

List of Figures

List of Tables

1 Introduction

Colorectal cancer (CRC) is one of the leading causes of cancer-related deaths Western countries (Loeve et al., 1999; Sung et al., 2021; Torre et al., 2015), and it is expected that the absolute number of cases will increase as a result of aging and growth of populations. Currently, the Dutch Rijksinstituut voor Volkgezondheid en Milieu estimates that one in twenty people will develop CRC in the Netherlands. Considerable research finds that CRC, or early stages thereof, can be detected and treated through population screening, which in turn could prevent a large proportion of CRC (death) cases. These findings raise the question: "which screening policies are best?".

Clinical trials often only last a couple of years, while policy makers are most interested in the (cost-)effectiveness of screening strategies over a lifetime. For example, to research whether CRC mortality can be reduced through changes in a current policy, one would have to follow individuals throughout their whole lives. Additionally, in order to compare amongst screening policies, one would have to simultaneously implement and evaluate multiple policies using a real-life population. Since both of these scenarios are infeasible in practice, the Erasmus Medical Center (EMC) developed the MISCAN-Colon (MIcrosimulaten SCreening ANalysis) model – a microsimulation model for the evaluation of CRC screening.

The current implementation of the MISCAN-Colon model at EMC follows the guidelines of the current screening procedure in the Netherlands. That is, each individual aged 55 to 75 years receives a faecal immunochemical test (FIT) once every two years, which can be performed at home on voluntary basis. This stool-based test measures the level of haemoglobin (blood) present in a patients faeces, where higher levels of blood may be related to polyps and CRC. Then, the MISCAN-Colon model uses the sensitivity (true positive rate) and specificity (true negative rate) of the FIT results to simulate a positive or negative FIT result for simulated individuals.

Recently, however, the Public Health department of EMC explored an extension of MISCAN-Colon to evaluate the benefits of personalised screening strategies, where instead of simulating FIT outcomes the model would simulate the haemoglobin concentrations in a patient's stool using an evolutionary linear mixed model algorithm (van Duuren et al., 2022). In this thesis, we use black-box machine learning methods as an alternative to this evolutionary algorithm to realise a second extension of the MISCAN-Colon model.

Most machine learning methods rely on the assumption of independently identically distributed observations, which is likely to be violated in healthcare data due to correlations within individuals[2]. To overcome this issue, Hajjem et al. (2014) propose an approach which incorporates random-effects in machine learning algorithms for efficient analysis of longitudinal data. Based on this approach, van den Berg (2021) finds that mixed-effect machine learning (MEml) models significantly outperform the current proposed method to simulate haemoglobin concentrations. The optimal MEml model was chosen to be a decision tree due to its interpretability, as more complicated models attained similar performance. It is unclear, however, whether the increase in predictive accuracy found in van den Berg (2021) is specif-

[2]In this case, patients with negative FITs participate in multiple rounds, which allows for such correlation.

ically due to the inclusion of random-effects, or due to the use of machine learning methods in general. Therefore, this research investigates the contribution of the inclusion of random-effects to the predictive accuracies of black-box machine learning methods. We implement artificial neural networks (ANNs) and eXtreme Gradient Boosting (XGBoost), both with and without mixed-effects, using the approach of Hajjem et al. (2014). This leads to the following research questions:

RQ1a Does the introduction of random-effects in machine learning models lead to better performance, i.e., do MEml models outperform 'regular' machine learning models?

RQ1b Which model is best suited for predicting the haemoglobin concentration based on the data set provided by EMC?

RQ2 How well does the model from Q1b perform as simulation model in MISCAN-Colon?

The data for this research is provided by the EMC from the Dutch national CRC screening program from 2014-2020. For each of the 3.2 million individuals in the data set, a maximum of four screening rounds are available. We only include individuals who participate in two or more *consecutive* rounds, and those who participate in one round in total. One of the variables in this data set is the current stage of CRC in an individual, which is imputed using the multiple imputation via chained equations approach by Van Buuren and Oudshoorn (1999).

This research consists of two phases, the first being outside of MISCAN-Colon, where we predict haemoglobin concentrations using five different models. These models are trained, validated, and tested using the longitudinal data set provided by the EMC. Based on phase one, we answer RQ1a and RQ1b. In phase two, we implement the most promising model in MISCAN-Colon, and calibrate this model such that the simulated haemoglobin concentrations resemble the observed concentrations of real-life Dutch population screening data as closely as possible. We then answer RQ2. The remainder of this research is structured as follows. We provide background information on colorectal cancer MISCAN-colon in Section 2, along with an overview of the applications of ANNs and XGBoost in healthcare literature. In Section 3 we describe the data and the data imputation method. We present our methodology in Section 4, followed by our results and conclusion in Sections 5 and 6 respectively.

2 Literature

2.1 Colorectal cancer

Colorectal cancer (CRC) is the development of cancer from the colon or rectum, which usually starts as a benign adenoma (i.e., a noncancerous tumor), and is one of the most commonly diagnosed and most deadly cancers worldwide (Torre et al., 2015; Sung et al., 2021). Specifically, according to the Dutch Rijksinstituut voor Volkgezondheid en Milieu five percent of people will develop CRC in the Netherlands. Nearly nine in ten cases of that 5% occur in people older than 55. Risk factors for CRC include age, gender, genetics, environment, diet, physical activity, and smoking (Botteri et al., 2008; Thanikachalam and Khan, 2019). Moreover, the worldwide burden of CRC is expected to further increase due to,

inter alia, the rapid growth and aging of the population (Jiang et al., 2022; Winawer, 2007), which is a testament to the importance of optimising screening procedures.

Only a small percentage of adenomas become cancerous (Strum, 2016). Therefore, we distinguish between progressive and non-progressive adenomas, where (non-)progressive adenomas do (not) develop into CRC, as shown in Figure 1. The most common form of CRCs are colorectal adenocarcinomas, with a prevalence of over 95% (Thrumurthy et al., 2016).

We also distinguish between clinical and preclinical stages, where preclinical indicates that the cancer is not yet diagnosed. Preclinical cancer can then progress from stage I to stage IV, where symptoms may develop in each stage, which in turn may lead to disease diagnosis (Compton and Greene, 2004). Once the cancer has been diagnosed as a result of symptoms, it is referred to as clinical.

Figure 1 shows the progression of CRC in five stages. In stage 0, the adenoma has not grown beyond the mucosa (i.e., the inner lining) of the colon or rectum. Stage I is when the cancerous adenocarcinoma has grown beyond the mucosa without spreading to the lymphatic system or distant organs. In stage II the adenomacarcinoma has invaded the colonic or rectal wall, with possible infection of nearby organs. Finally, in stages III and IV, the metastatic adenocarcinoma has spread to lymph nodes and distant organs.

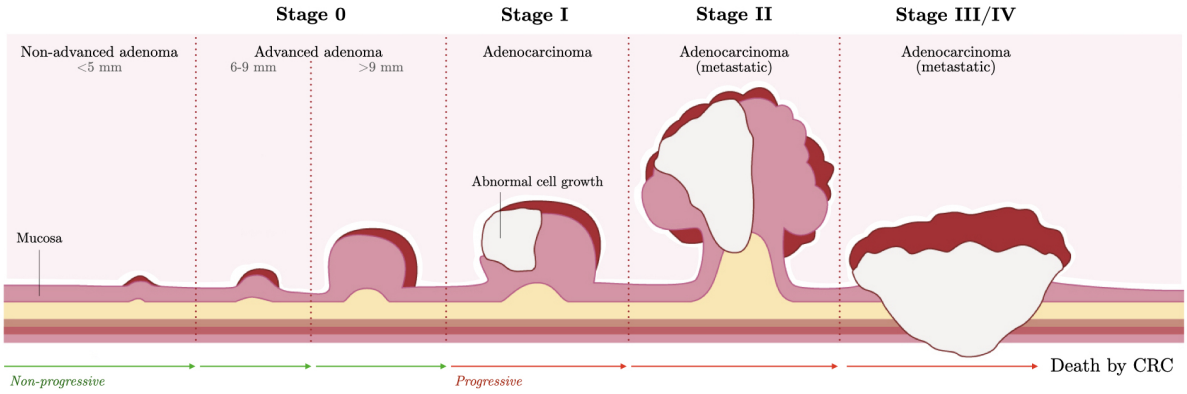

Figure 1: Progression of colorectal cancer in stages

2.1.1 Screening

The effect of screening is twofold. First, research indicates that over 90-95% of CRCs develop from (benign) adenomas (Bronner and Haggitt, 1993; Morson, 1974). Hence, early detection and removal of adenomas might aid in CRC prevention (Loeve et al., 1999). Second, early detection of an (a)symptomatic adenocarcinoma may result in an improvement in prognosis. Both of these findings are supported by, amongst others, Jiang et al. (2022); Levin et al. (2008); Toribara and Sleisenger (1995) and Whitlock et al. (2012).

Screening tests can be subdivided into two categories: stool-based tests and visual exams. The guaiac-based fecal occult blood test (gFOBT) and fecal immunochemical test (FIT), e.g., belong to the first category, in which the stool is tested for haemoglobin. If these tests report a high haemoglobin

concentration, this could be an indicator for the presence of CRC[3]. The two most common visual exams are (flexible) sigmoidoscopy, and colonoscopy, which investigate the structure of the colon and rectum for abnormal tissue. According to the review by Ding et al. (2022), colonoscopies are most effective in reducing CRC-related deaths at an approximate 68% decrease (Brenner et al., 2014). As for the stool-based tests, the FIT reduces CRC-related deaths by 22% on average, which is approximately 7% more effective than the gFOBT test (Hewitson et al., 2008; Zorzi et al., 2015). The FIT also has a higher participation rate and positivity rate compared to gFOBT in CRC screening programs, while reporting fewer false negatives (Mousavinezhad et al., 2016). Moreover, the FIT is relatively close in effectiveness compared to flexible sigmoidoscopies while being considerably less invasive, with reported mortality reduction of approximately 28%, (Holme et al., 2013). When screening with a test (other than a colonoscopy) leads to abnormal test results, defined as haemoglobin values above a fixed threshold, the general advice is to proceed with a follow-up colonoscopy (Ding et al., 2022).

In the Netherlands, each person between the age of 55-75 is asked to participate in the population screening for CRC once every two years since January of 2014[4]. The participants receive a FIT, which is sent back to the laboratory after taking a stool sample. If the sample exceeds the predetermined threshold of 47 micrograms haemoglobin per gram of faeces, health care professionals can make a referral for a colonoscopy and treatment. If any abnormalities are present during the colonoscopy, small amounts of tissue can be removed for analysis (i.e., a biopsy) and abnormal growths or adenomas can be identified and removed. This way, CRC can be detected at an early stage. Figure 2 shows that, according to the Integraal Kankercentrum Nederland, patients diagnosed with CRC through the Dutch population screening had a more favorable stage distribution than patients without screening. Also, patients who were diagnosed through population screening were more likely to receive less invasive treatments.

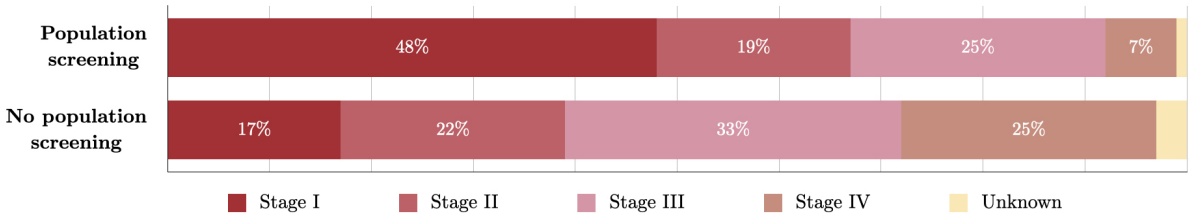

Figure 2: Distribution of diagnosed cancers in patients with, and without screening (source: https://iknl.nl/)

Unfortunately, screening is not a silver bullet in healthcare, as it could lead to, e.g., overdiagnosis or false positives, while also being costly and invasive. Welch and Black (2010) provide a summary of current evidence that early detection leads to overdiagnosis in breast, lung, and prostate cancer. Overdiagnosis – defined as the diagnosis of a medical condition or disease that would not cause symptoms or death during a patient's lifetime – is associated with long-term psychosocial harm, lower quality of life, and unwanted/unnecessary usage of (follow-up) tests, treatment, and healthcare facilities (Barton et al., 2001;

[3]Intestinal abnormalities, which may progress to cancer over time, bleed more than normal tissue. Thus, if a patients blood contains high haemoglobin concentrations, this might be an indication for (early stages of) CRC.

[4]For more information see: https://www.rivm.nl/darmkanker.

Brodersen and Siersma, 2013; Jenniskens et al., 2017; van der Steeg et al., 2011). On the other hand, Brasso et al. (2010) and Wardle et al. (2003) find no adverse psychological effects due to cancer screening, although they do not specifically investigate the effects of overdiagnosis. That said, overdiagnosis could be particularly harmful if it leads to unnecessary treatments, each of which comes with their specific risk[5].

Given the previously stated disadvantages to screening, it is clear that policy makers must continually evaluate the trade-off between harms and benefits to attain the most efficient screening policies. A large body of literature indicates that personalised screening may aid in achieving such optimized policies, e.g., for diseases such as colorectal-, prostate-, and breast cancer (Frampton et al., 2016; Pashayan et al., 2011; Schröder et al., 2009). Moreover, Grobbee et al. (2017) suggest that FIT-based programs can be improved upon by using a screening policy with person-specific intervals and -thresholds depending on previous haemoglobin concentrations in a person's stool. Particularly, haemoglobin concentrations just below the threshold are associated with higher risks of advanced neoplasia – a finding which can be exploited in personalised screening.

However, since personalised screening necessitates policymakers and health care providers to make decisions on, i.a., what tools to use to identify risk levels and at which risk levels screening or prevention programs are warranted, the possibilities of feasible personalised screening policies are limitless. Recently, van Duuren et al. (2022) addressed this problem using the adapted version of Habbema et al.'s (1985) MISCAN (MIcrosimulaten SCreening ANalysis) microsimulation model, called MISCAN-Colon, where one can overlay screening scenarios on a simulated population *before* real-life enforcement. The current implementation of the MISCAN-Colon model only simulates a positive or negative FIT result based on the sensitivity and specificity, but was extended by van Duuren et al. (2022) with a prototype module which returns haemoglobin concentrations in a person's stool.

2.2 Methods

This paper extends (part of) the research of van Duuren et al. (2022), using black-box machine learning methods instead of their linear mixed-effects model. However, as mentioned previously, oftentimes healthcare data is longitudinal, with (possibly) repeated measurements over different intervals of time, which could cause correlations within patients. Unfortunately, most machine learning methods are not robust to such correlations.

One possible solution to this problem could be to employ 'regular' machine learning models while explicitly modeling the interpatient correlation through inclusion of time-specific variables (e.g., current number of test, previous haemoglobin concentrations, maximum haemoglobin concentrations). However, the nature of this data suggests that better estimation may be possible if the information of the repeated measurements would be included at the level of the algorithm itself. In this section, we provide an overview of the literature on machine learning methods – specifically artificial neural networks (ANNs) and eXtreme Gradient Boosting (XGBoost) – in longitudinal health data.

[5]For an assessment of operative risk in CRC surgery, we refer to Fazio et al. (2004) and Hanley (2005).

2.2.1 Artificial neural networks

The trajectory of cancer is clearly non-linear, highly variable and dependent on a large variety of factors, most of which are not understood to this day. The flexibility of ANNs can be used to effectively address these problems. Another important property of ANN, with respect to our application, is their suitability for prediction of non-negative variables (Haghani et al., 2017; Sakthivel and Rajitha, 2017). Moreover, Haghani et al. (2017) shows that ANNs outperformed Poisson regression, negative binomial regression, zero-inflated Poisson regression, and zero-inflated negative binomial regression in their research to predicting the number of return to blood donations using zero-inflated data.

However, ANNs make the implicit assumption of independently identically distributed data, which is often violated in longitudinal data. While certain ANNs have been successfully adjusted to account for temporal trends (e.g., Choi et al.'s recurrent neural networks), longitudinal data often also contains unequal time intervals between measurements, and an unequal number of observations per individual. To account for these specific data characteristics, Xiong et al. (2019) propose a new type of ANN called the mixed effects neural network model, which adapts mixed effects within a deep neural network architecture for gaze estimation based on eye images. This model is person-specific, and uses few calibration samples to eliminate the person-specific bias in longitudinal data. In the field of Alzheimers, Tandon et al. (2006) introduce another mixed effects neural network to accurately model the nonlinear course of the disease. Their model generalizes a linear mixed effects model by incorporating a general non-linear function of the input variables. This model is shown to be much more accurate and effective compared to standard ANNs and linear mixed effects models. Lastly, Mandel et al. (2021) propose a generalized neural network mixed effects model, which is structured as a generalized linear mixed model (GLMM), where the linear fixed effect is replaced by a feed-forward ANN and a random effect component is added. They use this approach to predict depression and anxiety levels of schizophrenic patients using longitudinal data.

2.2.2 XGBoost

TO DO: XGBoost en zero-inflated data?

Tree-based algorithms The first to extend regression trees to longitudinal data was Segal (1992), who based his methodology on modifying the split function to accommodate repeated measures. This method, however, cannot handle time-varying covariates, and the resulting trees cannot be used to predict future periods for the same objects. Consequently, Sela and Simonoff (2011) propose a new method, the random effects expectation maximization (RE-EM), which accounts for the structure of longitudinal data and allows for prediction of future time periods and unbalanced panels. Hajjem et al. (2011) propose a comparable method to RE-EM, the mixed effects regression tree (MERT), which also first fits a tree without random effects and then updates the estimates with random effects until convergence. Although both RE-EM and MERT can appropriately deal with the possible random effects of observation-level covariates – in contrast to Segal (1992) – neither one of these methods allow for non-Gaussian data. To this end, following the steps of GLMM, Hajjem et al. (2017) propose a tree based approach that is

suitable for non-Gaussian data and can incorporate observation-level covariates and their potential random effects, called generalised mixed effects regression tree (GMERT). This extension uses the penalized quasi-likelihood method and expectation maximization for the estimation and computation, respectively. When the random effects are non-negligible, RE-EM, MERT, and GMERT each outperform regression trees without random effects based on both real-world and simulated data (Hajjem et al., 2011, 2017; Sela and Simonoff, 2011). Ngufor et al. (2019) also propose a model which integrates the random-effects structure of GLMM in non-linear machine learning models. Specifically, they combine the RE-EM estimation method proposed by Sela and Simonoff (2011) with the structure of the GMERT model of Hajjem et al. (2017) to predict longitudinal change in hemoglobin. Their proposed mixed-effects machine learning (MEml) method can use random forests, model-based recursive partitioning, conditional inference trees, or a gradient boosting machine. For an elaborate review on the (mathematical) similarities and difference between these models, see Appendix B.

Boosted tree-based algorithms One way to improve predictions in machine learning is through ensemble methods, such as XGBoost (Chen and Guestrin, 2016). The premise of boosting is to sequentially add weak base classifiers and iteratively adjusting the weighting of each base learner according to misclassifications to eventually create a single strong classifier. The consensus on the superior performance of ensemble methods has inspired many boosted alternatives to existing algorithms such as, e.g., boosted (non)-linear mixed-models (Griesbach et al., 2021; Sigrist, 2020; Tutz and Groll, 2010), boosted additive mixed-models (Groll and Tutz, 2012), and boosted poisson regression (Lee, 2021).

The emergence of boosted *tree-based* algorithms has only recently begun in longitudinal health care data. As most machine learning algorithms, XGBoost relies on the iid assumption, and its performance is highly dependent on the chosen training data in case of violation of this assumption. However, some researchers continue to employ machine learning approaches without taking (possible) violations into account. For example, Ryu et al. (2020) employ XGBoost using a combination of cross-sectional and longitudinal data to predict dementia risk[6], but they completely disregard the possibility of confounding effects of between-subject variability, which could lead to misleading inference (Ngufor et al., 2019). Additionally, they could be wasting an opportunity to achieve increased performance through capturing temporal relations in the data. In similar fashion, Moore and Bell (2022) compare myocardial infarction predictions of XGBoost to logistic regression using panel data, without any notion of the (possible) violation of the iid assumption[7].

That said, according to Dundar et al. (2007), violation of the iid assumptions should not matter much if the temporal dependency between samples is very weak and each sub-population occurs with highly similar frequency. For example, it might not be necessary (or even beneficial) to explicitly account for temporal dependencies at the level of the algorithm itself in a setting similar to Panchavati et al. (2022), who compare the infection predictions of hospitalized patients using machine learning methods (including XGBoost). That is, although they use longitudinal data, the data is collected over a short

[6]They combine the open source OASIS-1 and OASIS-2 data, which is advised against by OASIS, thus their analysis might contain more flaws in data processing than discussed here.

[7]It should be noted that this is a working paper, which has not been peer reviewed.

period of time – six hours – so it might be acceptable to assume no temporal dependencies are present between observations[8].

In contrast to the aforementioned papers, Wu et al. (2022) developed an algorithm to incorporate mixed-effects in longitudinal data. They use a growth mixture model to identify latent categories, considering individual and population heterogeneity. Once each trajectory is defined, any machine learning model can be used to predict within these trajectories. In their specific application, they find that XGBoost had the best performance. Chowdhury and Tomal (2022) propose a comparable framework which divides a complex multivariate problem into several univariate problems using observed time points, after which they employ multiple statistical and machine learning models to obtain marginal and conditional models as base learner. They also propose to include a lagged dependent variable as covariate to incorporate temporal dependencies. Although they do not employ XGBoost in specific, this could be easily implemented. Thus, both methods extend algorithms developed for cross-sectional data to predict risk trajectories for repeated responses.

Only few of the aforementioned methods are widely available in commonly used statistical software packages[9]. Since the employed method needs to be able to process both XGBoost and ANN to enable comparisons between both machine learning models, this research employs MERF. For a more elaborate discussion on this decision based on relative performance, mathematical properties, and compatibility, see Appendix B.6.

2.3 MISCAN-Colon

As previously mentioned, MISCAN-Colon allows for the evaluation of different screening policies by comparing their costs and effectiveness, as well as assessing the risk of false positives and overdiagnosis on a simulated population (Loeve et al., 1999).

The model simulates individual life histories in which several colorectal lesions can emerge, and produces incidence and mortality rates in the simulated population using information on the epidemiology and natural history of the disease as input combined with screening- and demography characteristics. By comparing the simulated life histories with, and without screening, MISCAN-Colon can evaluate the costs and benefits of a specific screening strategy.

The MISCAN-Colon model can be decomposed into three parts: demography, natural history and screening. Figure 3 shows an exemplified version of these three parts, using a fictive individual named Robin. The upper line, referred to as the demography part, simulates the life of Robin without cancer who dies at 87 years old of other causes than CRC. The middle line simulates Robin's life *with* cancer, but without screening, which adds a natural history of the disease to the demography part. In this scenario, Robin dies at 72 due to CRC. The bottom line simulates Robin's life when screening is overlayed, with 15 life years gained as a result.

[8] They do include the summary statistics of all values measured in the data set as covariates for continuously measured features in XGBoost, which might capture (some of) the correlation if present after all.

[9] Click here for the code/documentation of RE-EM, MERF, and MEml. An adapted version of MERT (namely stochastic MERT) is available here.

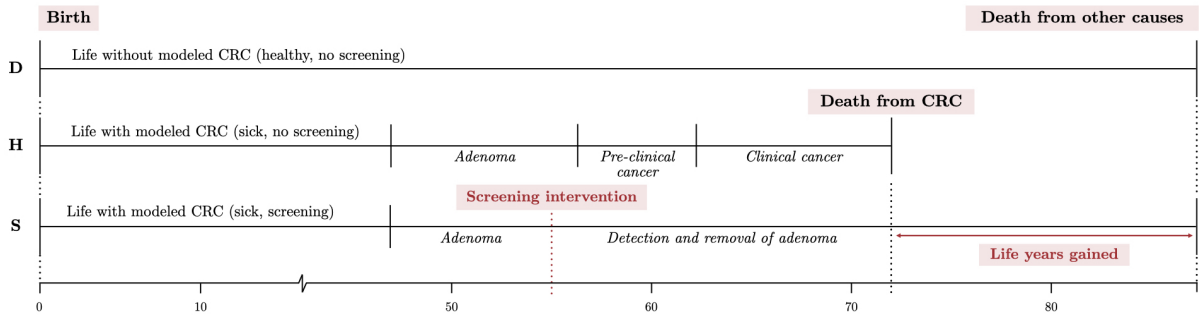

Figure 3: Simulations from the MISCAN-Colon model, where the upper bar shows the demography part (D), the middle bar adds the natural history (H) to D, and the lower bar adds both screening (S) and H to D

Three remarks on Figure 3. First, the survival of a lesion after diagnosis depends on the stage of the cancer (and other risk factors). Thus, screening does not ensure that an individual survives from CRC. The possible prognoses after a positive test result for CRC screening are: delay in moment of death, no change in moment of death, or premature death by complications of treatment. Second, the figure only shows examples of individuals with *one* lesion for simplicity, but the MISCAN-Colon model also allows for the modelling of zero or multiple lesions. New lesions that appear after clinical diagnosis of CRC are accounted for in the simulated survival. Third, Figure 3 only shows lethal progressive adenomas, but it is also possible that an individual develops non-lethal adenomas which would never result in death of an individual.

3 Data

The data for this research is obtained from the Dutch CRC screening program in 2014-2020. For each individual who participated in the biennial screening a maximum of four rounds of data are available. This analysis exclusively focuses on those who participated in one round only, or multiple consecutive rounds.

Given that this research explores, i.a., 'regular' machine learning models while within individual correlation might be present, we introduce additional variables to allow for as much individual variation as possible. Inspired by Chowdhury and Tomal (2022), we include a lagged dependent variable as covariates (previous haemoglobin concentrations), both to incorporate temporal dependency between the haemoglobin values of an individual, and because Grobbee et al. (2017) find that an undetectable haemoglobin concentration two years ago decreases the current risk of having CRC. We also include the minimum and maximum haemoglobin value per individual over all FITs prior to the current time of screening.

Table 1: Original variables in the data set provided by the Erasmus Medical Centre

Variable	Description	Range
`Age`	Age of respondent at time of screening	55 – 77
`Birth year`	Year of birth	1938 – 1963
`FIT number`[1]	Indicator for sequence number of the FIT	1 – 4
`Haemoglobin current`	Haemoglobin value found in FIT in current round	0 – 437.1
`Haemoglobin max`	Maximum obtained haemoglobin value over all tests at time of screening	0 – 47.0
`Haemoglobin min`	Minimum obtained haemoglobin value over all tests at time of screening	0 – 47.0
`Haemoglobin previous`	Haemoglobin value of previous round	0 – 47.0
`Haemoglobin threshold`	Threshold value used to determine the unit of the bloodtest result	275, 47
`ID`	Personal identification number	1 – 3,710,672
`Result`	Indicator for result of screening bloodtest	0 (Favourable, 96.1%), 1 (Unfavourable, 3.9%)
`Round`	Indicator for current round	1 – 4
`Sex`	Gender of respondent	0 (Male, 48.0%), 1 (Female, 52.0%)
`Stage`[2]	Stage of cancer at time of screening	1 (Healthy, 0.8%), 2 (Non-advanced adenoma, 1.1%), 3 (Advanced adenoma, 1.7%), 4 (Colorectal cancer, 0.3%), NA (Unknown, 96.1%)

Notes: [1]`Fit number` is one-hot encoded, such that the resulting dummy variables are equal to one for the current FIT, and zero otherwise.[2]`Stage` is only available for individuals where cancer has been detected, and is unknown otherwise.

After data pre-processing (described in Appendix A), the data set contains 6,796,731 observations for 3,170,234 individuals of which almost 52% are female. In total, 803,651 individuals participated in one round only, 1,108,079 individuals participated in two consecutive rounds, 1,118,003 individuals participated in three consecutive rounds, and 140,501 individuals participated in all four rounds. Table 1 shows an overview of all variables included in the data set, along with descriptive statistics. Figure 4a shows the distribution of haemoglobin concentration in the data set over all observations, and Figure 4b shows the distribution of haemoglobin concentrations amongst observations with positive FITs. Clearly, the dependent variable is heavily zero-inflated. We can also distinguish a bimodal distribution in the positive FITs, with the largest peak between $[47; 80]$ and a second peak around $[180; 260]$.

Figure 4: Haemoglobin concentration densities and histogram

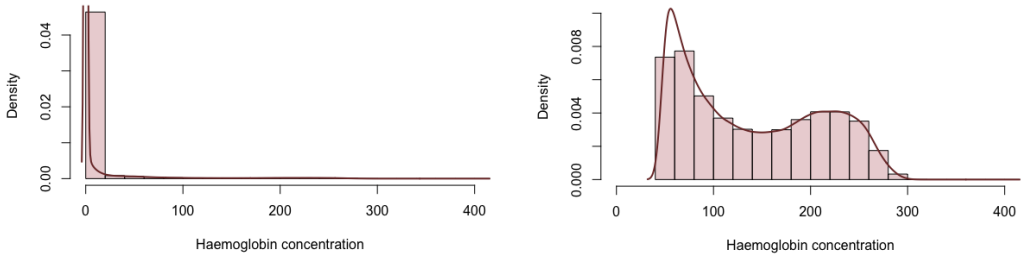

(a) Complete data set (in μg/g)

(b) Exclusively positive FITs (in μg/g)

3.1 Missing values

The `stage` variable is unknown for individuals with negative (favourable) FIT outcomes in phase one, as these individuals do not undergo follow-up procedures. In our data set 96.1% of observations report favourable FIT outcomes, such that `stage` is only known 3.9% of the time.

Most statistical procedures are designed for complete data, and ANNs are no exception to this rule. There are adaptations to ANNs to account for missing values, e.g., the combination of deep networks with probabilistic mixture modes by Śmieja et al. (2018). This method is based on the premise that instead of calculating the activation function on a single data point, the first hidden layer in the network computes the *expected* activation of neurons. XGBoost on the other hand is apt to handle sparse data through *sparsity-aware split finding*, which, in short, assigns a default direction of the branch if a sample's feature is missing and a decision node splits on that feature, such that the path can continue (Chen and Guestrin, 2016). However, this built-in algorithm is unlikely to perform well with the large number of missing values in our data. Moreover, if we were to employ the adapted ANN and XGBoost, we would not be able to validate whether the difference in performance between both models is a result of the models themselves or due to the inherent method of data processing. Thus, we are left with two options: either deleting or imputing `stage`.

If we only delete observations without reported stages, the resulting data set exclusively contains individuals above the cut-off value of 47 micrograms of haemoglobin per gram of faeces, which is not only unrepresentative for the Dutch population, but will also likely result in poor predictive performance when the models are used in MISCAN-Colon, where individuals below the cut-off do occur. A similar problem of decreased performance might also prevail when deleting the variable in its entirety, as previous internal research by EMC shows that `stage` is a strong predictor of haemoglobin concentrations. Additionally, as the purpose of screening is to identify the current stage of cancer in an individual, we opt to impute `stage`.

We include two additional data sets – the '15 threshold' and 'MISCAN simulation' data set – in an attempt to increase the accuracy of the imputations. The '15 threshold' data set, provided by the EMC from the Dutch national CRC screening program, contains a total of 16,591 individuals who participated in the first round of 2014[10] with known `stage`. The threshold for whether one should be admitted to the follow-up program was set to 15 micrograms of blood per gram of feces instead of 47 μg/g for a subset of these individuals. Thus, this data set contains real-life data on the current stage of individuals with `current haemoglobin` below 47 μg/g, in contrast to the original data set, which only reports `stage` for observations over 47 μg/g.

Given that the '15 threshold' data set is relatively small in size compared to the original data set, we also perform a population simulation run in MISCAN-Colon. Specifically, we simulate two million individuals from 2014-2020, with the same sex ratio as the original data set. This 'MISCAN simulation' data set consists of 3,076,778 observations, where the current `stage` is always known and `haemoglobin current` is always unknown. Table 6 in Appendix A.1 reports descriptive statistics for both additional

[10]The threshold was set to 47 μg/g for all individuals from round two in 2014 onward.

data sets. The combination of all three data sets results in 9,890,100 observations in total, of which 6,533,768 `stage` observations and 3,076,778 `haemoglobin current` observations are missing.

There are two major iterative approaches for multiple imputation in general missing data patterns: joint modeling and the fully conditional specification. Joint modeling assumes joint multivariate normality of all variables, which is inapt for imputing categorical variables, and therefore unsuitable for this analysis. In contrast, the fully conditional specification does not rely on multivariate normality, and applies a multivariate imputation model variable by variable using a collection of conditional densities per incomplete variable (Van Buuren, 2018).

A popular data imputation method amongst the fully conditional specification is Multiple Imputation via Chained Equations (MICE), which is an often used and recommended method in healthcare literature (Ambler et al., 2007; Baneshi and Talei, 2011; Chowdhury et al., 2017; Faris et al., 2002; Jolani et al., 2015). We employ MICE to impute `stage`, using `haemoglobin` `current`, `result`, `age`, and `sex`. To this end, we assume that the missing observations are missing at random, which means that there might be systematic differences between the missing and observed stages, but these can be entirely explained by other observed variables (Bhaskaran and Smeeth, 2014). In this case, the missingness of `stage` is a direct result of the test outcome of the FIT.

In each iteration of MICE we first impute `haemoglobin` `current`, and then impute the corresponding `stage`. Specifically, in step one, we replace all missing values in the data set with a random draw from the data as temporary place holder. In step two, we set the place holder back to missing only for the variable we wish to impute. In step three, we replace these missing values using an appropriate imputation method (e.g., sampling, predictive mean matching, linear regression or logistic regression) using (part of) the remaining variables in the data set. Steps two and three are then repeated until all missing variables are filled, at which point we completed one full cycle. We perform ten cycles in total, as per recommendation of Raghunathan et al. (2002). The observed data combined with the imputed values at the end of the tenth cycle constitute one imputed data set. This process is repeated to create 5 imputed data sets, such that a total of 5×10 iterations are performed. The final distribution of all five imputed versions of `stage` are then compared to the `stage` distribution in the 'MISCAN simulation' data set. The imputed variable which most closely compares to the MISCAN `stage` variable is then used as replacement for the *stage* variable in the original data set. As a final step, all observations from the '15 threshold' and 'MISCAN simulation' are removed. Appendix A.1 provides a more detailed explanation of the MICE algorithm specific to this paper.

4 Methodology

4.1 Machine learning

4.1.1 Artificial neural networks

ANNs, developed by Lippmann (1987), are inspired by the human brain, mimicking the way that biological neurons signal to one another. ANNs are comprised of (1) an input layer, (2) possibly one or more hidden

layers, and (3) an output layer. The input variables are related to the output variable(s) through a network of interconnected nodes, with associated weight and threshold. If the output of any individual node is above the specified threshold value, that node is activated, sending data to the next layer of the network. The optimal values for these weights are estimated when the ANN is fitted, such that a predetermined loss function is minimized – the mean squared error in our case. The input layer of the ANN consists of p nodes, where p is equal to the number of explanatory variables. In our setting, the output node $\hat{f}(x)$ represents the predicted haemoglobin concentration.

To advance from one layer to another, the ANN uses activation functions $h(\cdot)$, with the sum of the weights and the intercept, referred to as the bias, as input. Since each activation function has unique properties, we cannot determine which one is best in advance. Therefore, we consider three different activation functions: the identity activation function $h(x) = kx$, with k a fixed constant, the rectified linear unit (ReLu) activation function $h(x) = \max(0, x)$, and the sigmoid activation function $h(x) = \frac{e^x}{1+e^x}$. If all layers in the ANN use the linear identity activation function, the whole network is equal to a single layer ANN with linear activation function. That is, this ANN can only capture linear relations in the data. The derivative of the identity activation function is constant, such that the gradient is not influenced by the input. In contrast, small changes of input in the zero-centered bell-shaped derivative of the non-linear sigmoid activation function creates large changes of output when the input is near 0. However, this activation function might lead to gradient saturation for very small or very large values. The ReLu activation function does not suffer from this "vanishing gradients" problem as long as the input is positive. It is also less computationally expensive compared to the sigmoid activation function.

Hornik et al. (1989) show in their universal approximation theorem that an ANN with at least one hidden layer, and a large enough number of neurons, can approximate any finite-dimensional Borel measurable function up to any arbitrary accuracy. In other words, an ANN with zero hidden layers can only represent linear functions, whereas we can approximate *any* function with a continuous mapping with finite spaces using an ANN with one hidden layer. In practice, however, a network with multiple hidden layers can be more efficient. Therefore, we also tune the number of layers. In case of an ANN with two hidden layers, with H nodes in the first layer and L nodes in the second, the values at each node are calculated as follows:

$$
\begin{aligned}
z_h^1 &= g\left(\sum_{j=1}^{p} w_{hj}^1 x_j\right) && \forall h \in \{1, \ldots, H\}, \\
z_l^2 &= g\left(\sum_{h=1}^{H} w_{lh}^2 z_h^1\right) && \forall l \in \{1, \ldots, L\}, \\
\hat{f}(x) &= g\left(\sum_{l=1}^{L} w_l^3 z_l^2\right), &&
\end{aligned}
$$

where x_j represents each of the input regressors, z_i^j represents the i^{th} node of the j^{th} hidden layer, and w_{ik}^j is the weight of node k on node i in hidden layer j. Figure 5 shows an example of an ANN with two hidden layers.

One of the risks of ANNs is that they tend to overfit on the training data. To mitigate overfitting,

we use the efficient early stopping regularization (Prechelt, 1998), and dropout in the hidden layer(s) (Srivastava et al., 2014).

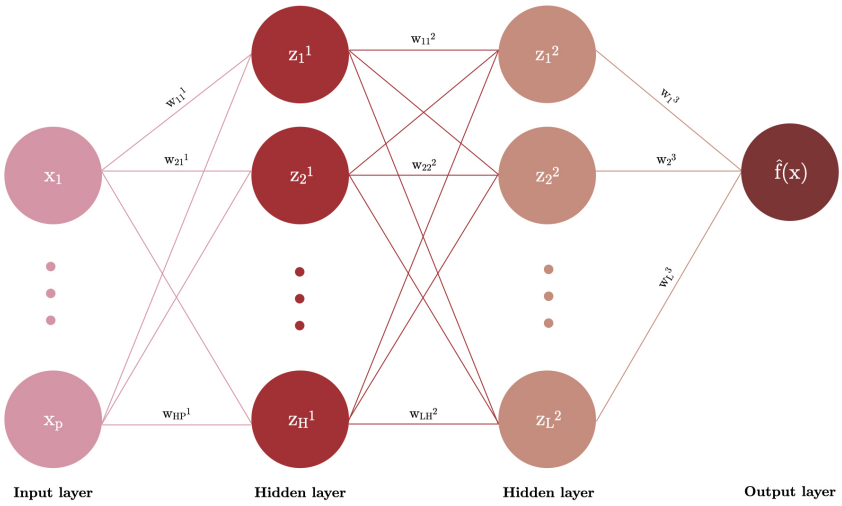

Figure 5: Example of an artificial neural network with two hidden layers and one output node

4.1.2 XGBoost

For our second method, we consider the scalable XGBoost algorithm. The idea is that the performance of current trees is improved upon by making more accurate predictions for observations for which the predictions of the previous trees are incorrect, such that each tree is dependent on its predecessor.

Adopting the notation of Chen and Guestrin (2016), the XGBoost algorithm minimizes a negative log-likelihood loss function that measures the difference between the prediction $E(y_i|x_i) = \hat{y}_i$ and the true outcome y_i for each individual, using a regularization term $\Omega(f_k)$. Specifically, the XGBoost regression algorithm minimizes the following objective function

$$\mathcal{L}(\hat{y}_i) = \sum_{i=1}^{N} l(y_i, \hat{y}_i) + \sum_{k=1}^{T} \Omega(f_k), \tag{1}$$

where $l(\hat{y}_i, y_i)$ is a differentiable convex training loss function and the regularization term equals $\Omega(f_k) = \gamma T + \frac{1}{2}\lambda\|\omega\|^2$ for $f_k \in (f_1, ..., f_T)$. The predicted values $\hat{y}_i$ are obtained by sequentially building shallow decision trees f_k, where the importance weights of every observation are updated proportional to their misclassification error in the previous tree. Each f_k corresponds to an independent tree structure q with leaf weights ω. The additional regularization term $\Omega(f_k)$ penalizes the complexity of regression tree f_k and consequently aids in the reduction of over-fitting. Just as for the ANN model, we use the (root) mean squared error as loss function. Instead of using traditional optimization methods to minimize the objective function in Equation 1, Chen and Guestrin (2016) propose to train the model in an additive manner. Let $\hat{y}_i^{(t)}$ be the i^{th} instance at the t^{th} iteration, we can rewrite the objective function as

$$\mathcal{L}^{(t)} = \sum_{i=1}^{N} l\left(y_i, \hat{y}_i^{(t-1)} + f_t\left(\mathbf{x}_i\right)\right) + \Omega\left(f_t\right), \tag{2}$$

where the algorithm greedily adds a tree f_t that most improves the model according to Equation 1. The rewritten objective function in Equation 2 is then optimized using second-order Taylor approximation. Thereafter, we can calculate the optimal weight of each leaf and the corresponding optimal value for fixed tree structures q[11].

TO DO: Overfitting komt nu een beetje uit de lucht vallen, iets meer over schrijven. To mitigate overfitting, we include a L2 regularization term on weights and we implement bagging through subsampling the training data and/or the features once in every boosting iteration.

4.2 Mixed-effects machine learning

As mentioned previously, although machine learning algorithms do not make *a priori* assumptions on the distribution of variables, they do often implicitly make the iid assumption on the regressors. To explore whether we can exploit the dependencies within individuals, we also model mixed-effects counterparts of ANN and XGBoost. Specifically, we use an adaptation to Hajjem et al.'s (2011) proposed mixed-effects framework, which follows the functional form:

$$\begin{aligned} y_i &= f\left(X_i\right) + Z_i b_i + \varepsilon_i \\ b_i &\sim N(0, D), \varepsilon_i \sim N\left(0, R_i\right) \\ i &= 1, \ldots, n, \end{aligned} \tag{3}$$

where the model for estimating the fixed-effects component, $f(X_i)$, is replaced by a machine learning model, inspired by Hajjem et al.'s (2014) extension of Hajjem et al. (2011). Since Hajjem et al. (2014) introduce their extension as a mixed-effects model solely to be used with random forests as machine learning model, this research contributes to the existing literature by using both ANN and XGBoost in this mixed-effects machine learning (MEml) framework instead.

The proposed MEml models are estimated using an expectation-maximization approach, in which the random effects in Equation 3, $Z_i b_i$, and the population-level effects, $f(X_i)$, are alternatively estimated. In essence, we first initialize the random effects $\hat{b}_i = 0$, and use this $\hat{b}_i$ to compute $y_i^* = y_i - Z_i \hat{b}_i$. We then train our machine learning model to estimate $\hat{f}(X_i)$, which is an estimate of $f(X_i)$ obtained from either an ANN or XGBoost model with y_i^* as responses and X_i as covariates. This process repeats until convergence of the generalised log-likelihood[12].

4.3 Tuning

As with most machine learning methods, the performance of both ANN and XGBoost are dependent on proper tuning. We cross-validate the hyperparameters of the different models using a Bayesian search called Hyperopt (Bergstra et al., 2013). This Hyperopt method can be seen as an exploration/exploitation strategy, that starts by exploring the performance across the candidate hyperparameter space, and subsequently randomly exploits the most promising subspace of hyperparameters.

[11] For a full mathematical formulation of these values, we refer to Chen and Guestrin (2016).
[12] For more details on the estimation procedure, we refer to Hajjem et al. (2011, 2014) and Appendix B.

Figure 6 shows a (simplified) illustration of Bayesian Hyperopt versus random grid search. The top two figures show that both methods start in the same manner by randomly exploring the candidate hyperparameter space. The bottom two figures show that, after a predetermined set of iterations, Hyperopt has switched to a guided search in seemingly promising subspaces in terms of cross-validated performance measures (the red region in the figure), whereas random grid search randomly continued through the search space. Bergstra et al. (2013) show that for the same number of iterations, their Hyperopt method can lead to better hyperparameter settings than the ones of random search[13].

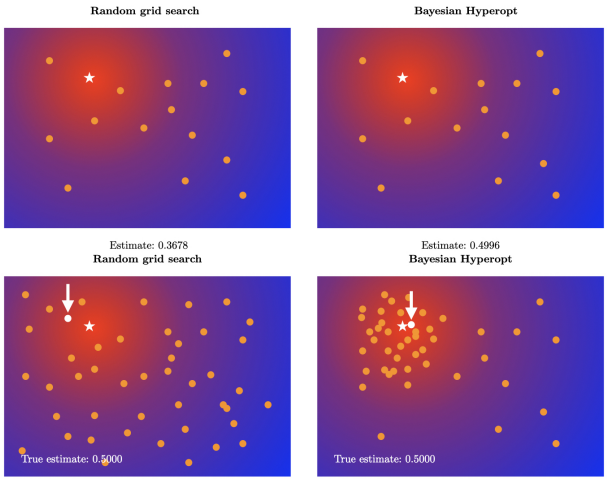

Figure 6: Random grid search versus Bayesian Hyperopt

The combination of parameters determines the allowed complexity of the model, whilst taking measures to prevent overfitting. For the (Me)ANNs, we tune the number of hidden layers, dropout rate per layer, activation function, number of neurons, batch size, and the learning rate. We do not consider weight decay since we already account for overfitting with early stopping and dropout. For the (Me)XGBoost models we tune the number of estimators, maximum tree depth, learning rate, L2 regularization term on weights, and the fraction of randomly selected training samples and features.

In addition, normalization might be necessary, as Jayalakshmi and Santhakumaran (2011) show that the performance of ANNs are contingent on normalization of the explanatory variables. **TO DO: citaat die dit ook vindt voor XGBoost** We consider four distinct normalization schemes: no normalization, min-max normalization, standardization, and robust standardization using the median and $25\% - 75\%$ interquantile range. For an overview of names, search spaces, and optimal values of each hyperparameter per model, see Appendix C.

[13]For computational efficiency one might also consider Putatunda and Rama's (2018) Randomized Hyperopt. This method first randomly samples a predetermined fraction $\phi \in [0, 1]$ from the validation train fold without replacement, and then performs a Hyperopt iteration on this sampled fold. In their application, they show that the loss in performance is limited, while drastically decreasing computation time, allowing for more Hyperopt iterations. However, due to the zero-inflated nature of our data, we opted against using randomised Hyperopt to ensure the dependent variable in each train fold follows a similar distribution distribution.

4.4 Forecasting

When making predictions outside of MISCAN-Colon, the models use age, sex, birth year, and FIT sequence number at time t, and the stage, and maximum, minimum, and previous haemoglobin value y_{t-1}^{Hb} at time $t-1$ to predict $\hat{y}_t^{Hb}$. We evaluate model performance on two test sets, the first consisting of observations of new individuals and the second consisting of observations of individuals the model has seen before. Our main focus is on the first test set, as the eventual goal of this analysis is to find a model that will perform best in the MISCAN-Colon implementation, which produces haemoglobin values of simulated individuals, which the model naturally has never seen before. However, seeing as the ability to distinguish between predictions for new and existing individuals is one of the strengths of the mixed-effects model, we also evaluate performance of all models on a test set with existing individuals as complementary analysis. To create these test sets, we first create a 70/30 train/test split where we ensure that each ID occurs only once between these two groups.

We then create four folds of the train group to perform stratified k-fold cross validation. Thus, we create four folds with a 75/25 train/validation split based on the distribution of haemoglobin.

We create two distinct groups of individuals to create the train, validation and test set. Group 1 is for training and validation, and group 2 is for testing. Thus, each ID occurs only once between these two groups.

TO DO: Zeggen dat predictions niet negatief mogen zijn en dat dat bij XGBoost wel kan gebeuren

4.5 Class imbalance

Since the data is zero-inflated, and therefore highly unbalanced, we considered using the state-of-the-art rebalancing techniques such as SMOTER (Torgo et al., 2013) or SMOGN (Branco et al., 2017), regression variants of (Chawla et al., 2002)'s widely-used Synthetic Minority Oversampling TEchnique (SMOTE). However, none of these methods take into account the longitudinal structure of the data. For example, when oversampling using SMOTER, we create synthetic points based on k-nearest neighbors. How should this synthetic point be interpreted? Is it a new individual? Is it an added observation for an existing individual? Is this point then representative for an observation 2 years later than the latest observation? Also, the more obvious apprehensions to over- and undersampling still hold, such as the fact that probability estimates will no longer be well calibrated.

TO DO: Discuss how ANNs have shown to work fine with zero-inflted data, see literature. XGBoost has not, therefore we consider running the XGBoost model with Tweedie loss objective as well. We cannot use Tweedie in the mixed-effects models because there the ml model is used to predict y*, not y, and we do not know the distribution of y*, thus we cannot determine whether it would be appropriate to use.

4.5.1 Tweedie loss

Given that the dependent variable in this research is heavily zero-inflated, we also explore using the Tweedie loss function described in Yang et al. (2018) as loss function $l(y_i, \hat{y}_i)$ in Equation 1, which can be written as

$$\begin{aligned} l\left(y_i, \hat{y}_i, \rho\right) &= \sum_{i=1}^{N} -y_i \frac{\exp\left[\log(\hat{y}_i)(1-\rho)\right]}{1-\rho} + \frac{\exp\left[\log(\hat{y}_i)(2-\rho)\right]}{2-\rho} \\ &= \sum_{i=1}^{N} -y_i \frac{\hat{y}_i^{(1-\rho)}}{1-\rho} + \frac{\hat{y}_i^{(2-\rho)}}{2-\rho}, \end{aligned}$$

where $\rho \in [1, 2]$ is the Tweedie power parameter. Tweedie distributions are a family of distributions that include gamma, normal, Poisson and their combinations. The power parameter, which is set to 1.6 in our research[14], allows the user to specify which mean-variance relation to use.

5 Results

The root mean squared error (RMSE), mean absolute error (MAE), and median absolute error (MedAE) are used to assess individual predictions. We also include the percentage correctly specified (PCC) and the percentage deviation (PDev), solely for the reader to make the results more intuitive. The PCC is based on a threshold of 47 μg/g, and reports the percentage of predictions that are below (above) this threshold when the true value is also below (above) this threshold. The PDev is based on a threshold of either 3 or 10 μg/g haemoglobin and indicates the percentage of predictions within the interval $[y_{true} \pm \text{threshold}]$.

TO DO: Discuss which models 'win' based on evaluation metrics: mexgboost and tweedieXGBoost

Table 2 shows that XGBoost provides the most accurate predictions above the threshold of 47μg/g. However, XGBoost is outperformed by each of the remaining models based on all other evaluation metrics in Table 4, and all statistics in Table 4. This higher percentage deviation might then be a result of the model predicting a larger proportion of observations above the threshold in general (see Figure 7a and 7c).

Table 4 shows the zero-inflation seems to be best captured by ANN and MeANN, based on their 5%, 10%, and 25% quantile being equal to that of the true data. This high density around zero also becomes evident from Figure 7a and 7b. On the other hand, Table 2 shows that both ANN and MeANN are outperformed on all evaluation metrics by (Me)XGBoost or TweedieXGBoost. Specifically, MeXGBoost attains the lowest RMSE and provides the most accurate predictions based on a $\pm 3\mu$g/g interval. TweedieXGBoost performs best as measured by the mean and median absolute error and accurately estimated the largest share of observations within a $\pm 10\mu$g/g interval of the true haemoglobin concentration. More-

[14] This number is based on an exploratory analysis first using one Hyperopt iteration (see Section 4.3), which resulted in two candidates: $\rho = 1.3 \wedge \rho = 1.6$, based on Tweedie loss and RMSE. We then chose $\rho = 1.6$ based on five Hyperopt iterations, as it provided more similar descriptive statistics of the predictions versus true values, and due to its much lower Tweedie loss. The RMSE's were similar for values of the power parameter.

over, Table 4 shows that the mean and 95% quantile of MeXGBoost predictions most closely corresponds to the original. TweedieXGBoost is most similar in the number of distinct values, median, and the 75% and 95% quantiles. The TweedieXGBoost model is also the only model to provide estimates over 300μg/g.

We use the modified Diebold-Mariano test whether the differences two forecasts are of statistical significance. Table 3 shows that the worst best model is MeXGBoost followed by TweedieXGBoost, ANN, MeANN, and XGBoost as worst performing model. All forecasts differ significantly, based on a 0.001 significance level.

Table 2: Evaluation metrics on test data

	ANN	**MeANN**	**XGBoost**	**MeXGBoost**	**TweedieXGBoost**
RMSE	28.2625	28.3576	29.7263	22.4086	22.9115
MAE	10.2057	10.1774	13.8937	6.9450	6.7224
MedAE	1.6	1.8	5.3	1.6	1.5
PCC	94.88%	94.94%	92.91%	97.33%	97.61%
PDev (3 μg/g)	60.80%	63.50%	38.02%	78.14%	77.58%
PDev_lb (3 μg/g)	63.09%	65.89%	39.41%	81.11%	80.54%
PDev_ub (3 μg/g)	2.09%	2.16%	2.40%	2.03%	1.82%
PDev (10 μg/g)	80.08%	81.94%	73.48%	88.34%	89.00%
PDev_lb (10 μg/g)	82.94%	84.87%	76.05%	91.52%	92.25%
PDev_ub (10 μg/g)	6.80%	6.85%	7.54%	6.79%	5.93%

Notes: This table shows the root mean squared error (RMSE), mean absolute error (MAE), median absolute error (MedAE), percentage correctly specified (PCC) and percentage deviation (PDev) for observations with true haemoglobin concentrations below 47 μg/g (PDev_lb) and above 47 μg/g (PDev_ub). The red colored cells denote the best performing model per model evaluation metric.

Table 3: Modified Diebold-Mariano test

	ANN	**MeANN**	**XGBoost**	**MeXGBoost**
MeANN	-16.6539^{*}			
XGBoost	-89.2453^{*}	-85.0188^{*}		
MeXGBoost	162.0751^{*}	168.8821^{*}	231.8874^{*}	
TweedieXGBoost	131.6228^{*}	135.4936^{*}	183.3655^{*}	-22.9475^{*}

Notes: This table shows the modified Diebold-Mariano test statistic, used to assess the relative performance between all models. A positive (negative) value indicates that the row (column) outperforms the column (row). An asterisk* denotes significance based on a significance level of 0.001.

Table 4: Descriptive statistics forecasts versus true haemoglobin concentration

	Distinct	**Mean**	**.05**	**.10**	**.25**	**Median**	**.75**	**.90**	**.95**	**Max**
Original	2975	6.397	0.0	0.0	0.0	0.0	0.0	3.6	29.4	318.0
ANN	1780	10.26	0.0	0.0	0.0	1.4	6.2	15.1	78.0	178.5
MeANN	1781	10.16	0.0	0.0	0.0	1.6	5.5	15.0	77.3	183.3
XGBoost	2125	14.62	0.1	1.0	2.0	5.1	10.1	36.4	81.5	246.4
MeXGBoost	2007	6.587	0.0	0.0	0.8	1.6	2.4	8.1	20.4	266.3
TweedieXGBoost	2192	5.915	0.2	0.2	0.7	1.4	2.2	7.5	16.9	358.7

Notes: This table shows the number of distinct values, mean, median, minimum, maximum, and the 5%, 10%, 25%, 75%, 90%, and 95% quantiles of the original dependent variable and its estimated counterpart of each model. The red colored cells denote the best performing model(s) per statistic.

Figure 7: Histograms of (predicted) haemoglobin concentrations in μg/g

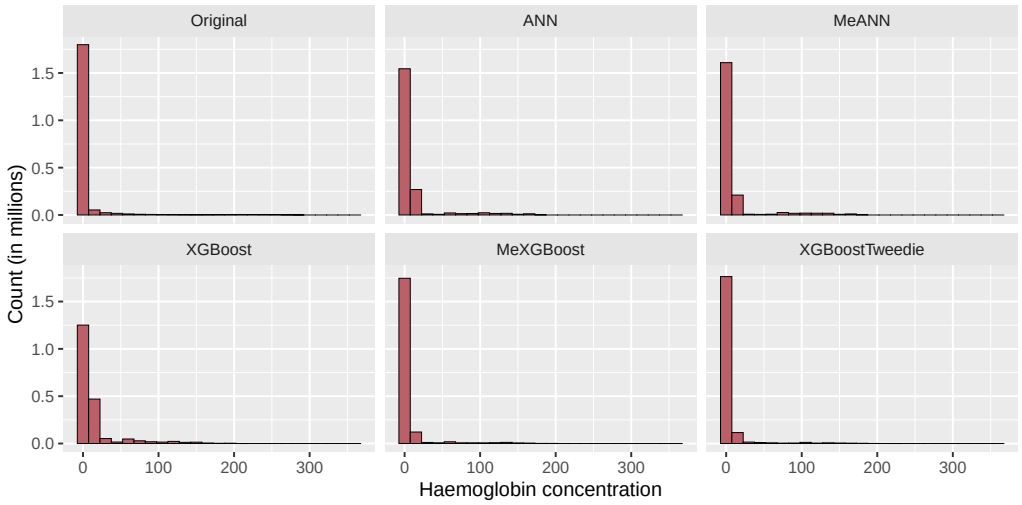

(a) Complete data set (in μg/g)

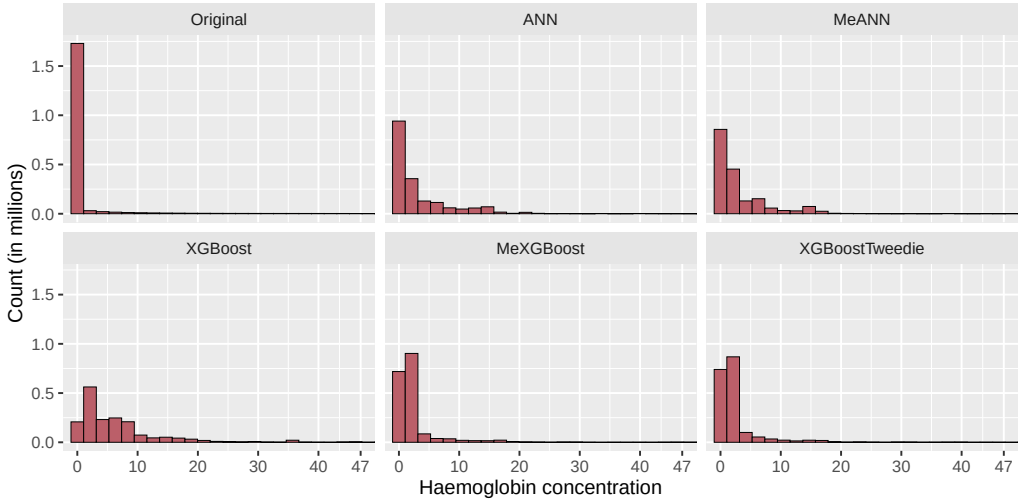

(b) Exclusively negative FITs (in μg/g)

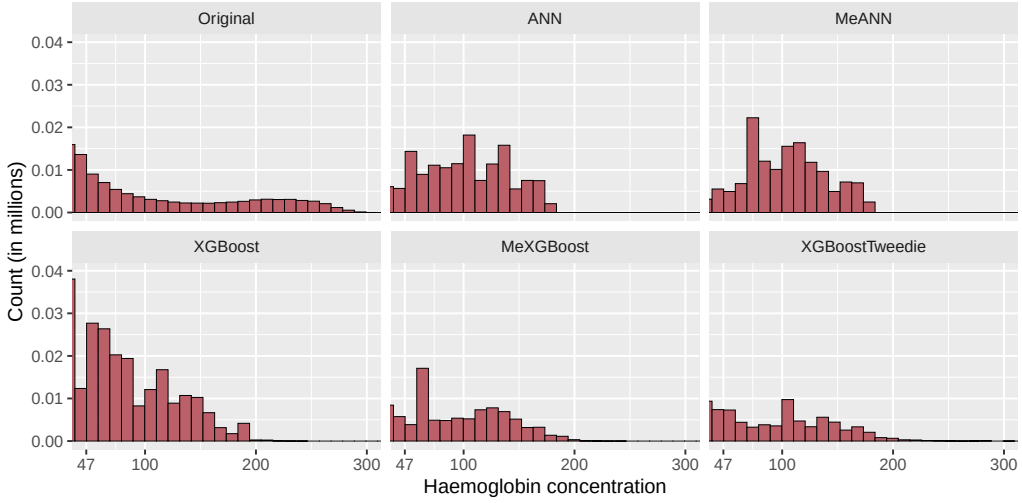

(c) Exclusively positive FITs (in μg/g)

TO DO: Cucconi test?

TO DO: Discuss which models 'win' based on distribution: mexgboost

The Kullback-Leibler divergence is an asymmetric measure of discrepancy between two distributions. Intuitively, in our case, the KL divergence is the information lost when the (Me)ML models are used to approximate the original distribution. A KL divergence of 0 indicates perfectly similar distributions. The divergence ranges anywhere from $[0, \infty]$. The Kolmogorov-Smmirnov test is an actual statistical test of the null hypothesis that two samples are drawn from the same distribution. Both KL divergence and the KS statistic are measures of similarity between distributions, though they have completely different properties in general.

Since the p-value is less than .05 for all models, we reject the null hypothesis of the KS test. Thus, there is no significant indication that either one of the forecasts come from the original distribution. The KL divergences do, however, indicate that our forecasts are not too bad, with the best value for MeXGBoost, which is in line with the conclusion drawn from the modified Diebold-Mariano test in Table 3. **TO DO: really poor description of the KL divergence outcome. What is a low value? what does the value even mean exactly?**

Table 5: Kolmogorov-Smirnoff test compared to original (unknown) distribution

	ANN	**MeANN**	**XGBoost**	**MeXGBoost**	**TweedieXGBoost**
Kullback-Leibler	1.7640	2.0045	2.2528	1.5459	1.9087
Kolmogorov-Smirnov	0.4598*	0.5906*	0.8246*	0.7624*	0.8708*

Notes: This table shows the Kolmogorov-Smirnov test statistic, where an asterisk denotes significance based on a significance level of 0.001, and the Kullback-Leibler divergence for each model, where the red colored cell denotes the best performing model per this metric.

Based on our previous discussion on the evaluation metrics, statistics, histograms, modified Diebold-Mariano test, and the Kullback-Leibler divergence, we choose to implement MeXGBoost in the MISCAN-Colon model in phase two of this paper.

6 Conclusion

References

Ambler, G., Omar, R. Z., and Royston, P. (2007). A comparison of imputation techniques for handling missing predictor values in a risk model with a binary outcome. *Statistical Methods in Medical Research*, 16(3):277–298.

Baneshi, M. and Talei, A. (2011). Multiple Imputation in Survival Models: Applied on Breast Cancer Data. *Iranian Red Crescent Medical Journal*, 13(8):544.

Barton, M. B., Moore, S., Polk, S., Shtatland, E., Elmore, J. G., and Fletcher, S. W. (2001). Increased patient concern after false-positive mammograms. *Journal of General Internal Medicine*, 16(3):150–156.

Bergstra, J., Yamins, D., and Cox, D. D. (2013). Hyperopt: A Python Library for Optimizing the Hyperparameters of Machine Learning Algorithms. In *Proceedings of the 12th Python in Science Conference*, volume 13, page 20. Citeseer.

van den Berg, D. (2021). Simulation of haemoglobin concentrations in MISCAN-Colon using a mixed-effect machine learning model. Master's thesis, Erasmus University Rotterdam.

Bhaskaran, K. and Smeeth, L. (2014). What is the difference between missing completely at random and missing at random? *International Journal of Epidemiology*, 43(4):1336–1339.

Botteri, E., Iodice, S., Bagnardi, V., Raimondi, S., Lowenfels, A. B., and Maisonneuve, P. (2008). Smoking and Colorectal Cancer: A Meta-analysis. *Journal of the American Medical Association*, 300(23):2765–2778.

Branco, P., Torgo, L., and Ribeiro, R. P. (2017). SMOGN: a Pre-processing Approach for Imbalanced Regression. In *First International Workshop on Learning with Imbalanced Domains: Theory and Applications*, volume 74, pages 36–50. Proceedings of Machine Learning Research.

Brasso, K., Ladelund, S., Frederiksen, B. L., and Jørgensen, T. (2010). Psychological distress following fecal occult blood test in colorectal cancer screening–a population-based study. *Scandinavian Journal of Gastroenterology*, 45(10):1211–1216.

Brenner, H., Stock, C., and Hoffmeister, M. (2014). Effect of screening sigmoidoscopy and screening colonoscopy on colorectal cancer incidence and mortality: systematic review and meta-analysis of randomised controlled trials and observational studies. *British Medical Journal*, 348.

Brodersen, J. and Siersma, V. D. (2013). Long-Term Psychosocial Consequences of False-Positive Screening Mammography. *The Annals of Family Medicine*, 11(2):106–115.

Bronner, M. P. and Haggitt, R. C. (1993). The Polyp-Cancer Sequence: Do All Colorectal Cancers Arise from Benign Adenomas? *Gastrointestinal Endoscopy Clinics of North America*, 3(4):611–622.

Capitaine, L., Genuer, R., and Thiébaut, R. (2021). Random forests for high-dimensional longitudinal data. *Statistical Methods in Medical Research*, 30(1):166–184.

Chawla, N. V., Bowyer, K. W., Hall, L. O., and Kegelmeyer, W. P. (2002). SMOTE: Synthetic Minority Over-sampling Technique. *Journal of Artificial Intelligence Research*, 16:321–357.

Chen, T. and Guestrin, C. (2016). XGBoost: A Scalable Tree Boosting System. In *Proceedings of the 22nd ACM SIGKDD International Conference on Knowledge Discovery and Data Mining*, pages 785–794. ACM.

Choi, E., Bahadori, M. T., Schuetz, A., Stewart, W. F., and Sun, J. (2016). Doctor AI: Predicting Clinical Events via Recurrent Neural Networks. In *Machine Learning for Healthcare Conference*, pages 301–318. Proceedings of Machine Learning Research.

Chowdhury, M. H., Islam, M. K., and Khan, S. I. (2017). Imputation of Missing Healthcare Data. In *20th International Conference of Computer and Information Technology*, pages 1–6. IEEE.

Chowdhury, R. I. and Tomal, J. H. (2022). Risk prediction for repeated measures health outcomes: A divide and recombine framework. *Informatics in Medicine Unlocked*, 28:100847.

Compton, C. C. and Greene, F. L. (2004). The Staging of Colorectal Cancer: 2004 and Beyond. *CA: A Cancer Journal for Clinicians*, 54(6):295–308.

Ding, H., Lin, J., Xu, Z., Chen, X., Wang, H. H., Huang, L., Huang, J., Zheng, Z., and Wong, M. C. (2022). A Global Evaluation of the Performance Indicators of Colorectal Cancer Screening with Fecal Immunochemical Tests and Colonoscopy: A Systematic Review and Meta-Analysis. *Cancers*, 14(4):1073.

Dundar, M., Krishnapuram, B., Bi, J., and Rao, R. B. (2007). Learning Classifiers When the Training Data Is Not IID.

Faris, P. D., Ghali, W. A., Brant, R., Norris, C. M., Galbraith, P. D., Knudtson, M. L., Investigators, A., et al. (2002). Multiple imputation versus data enhancement for dealing with missing data in observational health care outcome analyses. *Journal of Clinical Epidemiology*, 55(2):184–191.

Fazio, V. W., Tekkis, P. P., Remzi, F., and Lavery, I. C. (2004). Assessment of operative risk in colorectal cancer surgery: the Cleveland Clinic Foundation colorectal cancer model. *Diseases of the Colon & Rectum*, 47(12):2015–2024.

Frampton, M., Law, P., Litchfield, K., Morris, E., Kerr, D., Turnbull, C., Tomlinson, I., and Houlston, R. (2016). Implications of polygenic risk for personalised colorectal cancer screening. *Annals of Oncology*, 27(3):429–434.

Griesbach, C., Säfken, B., and Waldmann, E. (2021). Gradient boosting for linear mixed models. *The International Journal of Biostatistics*, 17(2):317–329.

Grobbee, E. J., Schreuders, E. H., Hansen, B. E., Bruno, M. J., Lansdorp-Vogelaar, I., Spaander, M. C., and Kuipers, E. J. (2017). Association Between Concentrations of Hemoglobin Determined by Fecal Immunochemical Tests and Long-term Development of Advanced Colorectal Neoplasia. *Gastroenterology*, 153(5):1251–1259.

Groll, A. and Tutz, G. (2012). Regularization for Generalized Additive Mixed Models by Likelihood-Based Boosting. *Methods of Information in Medicine*, 51(02):168–177.

Habbema, J., van Oortmarssen, G., Lubbe, J. T. N., and van der Maas, P. (1985). The MISCAN simulation program for the evaluation of screening for disease. *Computer Methods and Programs in Biomedicine*, 20(1):79–93.

Haghani, S., Sedehi, M., and Kheiri, S. (2017). Artificial Neural Network to Modeling Zero-inflated Count Data: Application to Predicting Number of Return to Blood Donation. *Journal of Research in Health Sciences*, 17(3):392.

Hajjem, A., Bellavance, F., and Larocque, D. (2011). Mixed effects regression trees for clustered data. *Statistics & Probability Letters*, 81(4):451–459.

Hajjem, A., Bellavance, F., and Larocque, D. (2014). Mixed-effects random forest for clustered data. *Journal of Statistical Computation and Simulation*, 84(6):1313–1328.

Hajjem, A., Larocque, D., and Bellavance, F. (2017). Generalized mixed effects regression trees. *Statistics & Probability Letters*, 126:114–118.

Hanley, J. A. (2005). Analysis of Mortality Data from Cancer Screening Studies: Looking in the Right Window. *Epidemiology*, pages 786–790.

Hewitson, P., Glasziou, P., Watson, E., Towler, B., and Irwig, L. (2008). Cochrane Systematic Review of Colorectal Cancer Screening Using the Fecal Occult Blood Test (Hemoccult): An Update. *Journal of the American College of Gastroenterology*, 103(6):1541–1549.

Holme, Ø., Bretthauer, M., Fretheim, A., Odgaard-Jensen, J., and Hoff, G. (2013). Flexible sigmoidoscopy versus faecal occult blood testing for colorectal cancer screening in asymptomatic individuals (Review). *Cochrane Database of Systematic Reviews*.

Hornik, K., Stinchcombe, M., and White, H. (1989). Multilayer Feedforward Networks Are Universal Approximators. *Neural networks*, 2(5):359–366.

Jayalakshmi, T. and Santhakumaran, A. (2011). Statistical Normalization and Back Propagation for Classification. *International Journal of Computer Theory and Engineering*, 3(1):1793–8201.

Jenniskens, K., De Groot, J. A., Reitsma, J. B., Moons, K. G., Hooft, L., and Naaktgeboren, C. A. (2017). Overdiagnosis across medical disciplines: a scoping review. *BMJ Open*, 7(12):e018448.

Jiang, Y., Yuan, H., Li, Z., Ji, X., Shen, Q., Tuo, J., Bi, J., Li, H., and Xiang, Y. (2022). Global pattern and trends of colorectal cancer survival: a systematic review of population-based registration data. *Cancer Biology & Medicine*, 19(2):175.

Jolani, S., Debray, T. P., Koffijberg, H., van Buuren, S., and Moons, K. G. (2015). Imputation of systematically missing predictors in an individual participant data meta-analysis: a generalized approach using mice. *Statistics in Medicine*, 34(11):1841–1863.

Kilham, P., Hartebrodt, C., and Kändler, G. (2018). Article generating tree-level harvest predictions from forest inventories with random forests. *Forests*, 10(1):20.

Laird, N. M. and Ware, J. H. (1982). Random-effects models for longitudinal data. *Biometrics*, pages 963–974.

Lee, S. C. (2021). Addressing imbalanced insurance data through zero-inflated Poisson regression with boosting. *ASTIN Bulletin: The Journal of the IAA*, 51(1):27–55.

Levin, B., Lieberman, D. A., McFarland, B., Andrews, K. S., Brooks, D., Bond, J., Dash, C., Giardiello, F. M., Glick, S., Johnson, D., et al. (2008). Screening and Surveillance for the Early Detection of Colorectal Cancer and Adenomatous Polyps, 2008: A Joint Guideline From the American Cancer Society, the US Multi-Society Task Force on Colorectal Cancer, and the American College of Radiology. *Gastroenterology*, 134(5):1570–1595.

Lippmann, R. (1987). An Introduction to Computing with Neural Nets. *IEEE ASSP magazine*, 4(2):4–22.

Loeve, F., Boer, R., van Oortmarssen, G. J., van Ballegooijen, M., and Habbema, J. D. F. (1999). The MISCAN-COLON Simulation Model for the Evaluation of Colorectal Cancer Screening. *Computers and Biomedical Research*, 32(1):13–33.

Mandel, F., Ghosh, R. P., and Barnett, I. (2021). Neural networks for clustered and longitudinal data using mixed effects models. *Biometrics: A Journal of the International Biometric Society*.

Mangino, A. A. and Finch, W. H. (2021). Prediction with mixed effects models: A monte carlo simulation study. *Educational and Psychological Measurement*, 81(6):1118–1142.

Moore, A. and Bell, M. (2022). XGBoost, a novel explainable AI technique, in the prediction of myocardial infarction, a UK Biobank cohort study. *medRxiv preprint*.

Morson, B. (1974). The polyp-cancer sequence in the large bowel. *Journal of the Royal Society of Medicine*, 67:451–457.

Mousavinezhad, M., Majdzadeh, R., Sari, A. A., Delavari, A., and Mohtasham, F. (2016). The effectiveness of FOBT vs. FIT: A meta-analysis on colorectal cancer screening test. *Medical Journal of the Islamic Republic of Iran*, 30:366.

Ngufor, C., van Houten, H., Caffo, B. S., Shah, N. D., and McCoy, R. G. (2019). Mixed Effect Machine Learning: A framework for predicting longitudinal change in hemoglobin A1c. *Journal of Biomedical Informatics*, 89:56–67.

Panchavati, S., Zelin, N. S., Garikipati, A., Pellegrini, E., Iqbal, Z., Barnes, G., Hoffman, J., Calvert, J., Mao, Q., and Das, R. (2022). A comparative analysis of machine learning approaches to predict C. difficile infection in hospitalized patients. *American Journal of Infection Control*, 50(3):250–257.

Pashayan, N., Duffy, S. W., Chowdhury, S., Dent, T., Burton, H., Neal, D. E., Easton, D. F., Eeles, R., and Pharoah, P. (2011). Polygenic susceptibility to prostate and breast cancer: implications for personalised screening. *British Journal of Cancer*, 104(10):1656–1663.

Prechelt, L. (1998). Automatic early stopping using cross validation: quantifying the criteria. *Neural Networks*, 11(4):761–767.

Putatunda, S. and Rama, K. (2018). A Comparative Analysis of Hyperopt as Against Other Approaches for Hyper-Parameter Optimization of XGBoost. In *Proceedings of the 2018 International Conference on Signal Processing and Machine Learning*, pages 6–10.

Raghunathan, T. E., Solenberger, P. W., and Van Hoewyk, J. (2002). IVEware: Imputation and Variance Estimation Software. *University of Michigan*.

Ryu, S.-E., Shin, D.-H., and Chung, K. (2020). Prediction Model of Dementia Risk Based on XGBoost Using Derived Variable Extraction and Hyper Parameter Optimization. *IEEE Access*, 8:177708–177720.

Sakthivel, K. and Rajitha, C. (2017). A Comparative Study of Zero-inflated, Hurdle Models with Artificial Neural Network in Claim Count Modeling. *International Journal of Statistics and Systems*, 12(2):265–276.

Schröder, F. H., Hugosson, J., Roobol, M. J., Tammela, T. L., Ciatto, S., Nelen, V., Kwiatkowski, M., Lujan, M., Lilja, H., Zappa, M., et al. (2009). Screening and Prostate-Cancer Mortality in a Randomized European Study. *New England Journal of Medicine*, 360(13):1320–1328.

Segal, M. R. (1992). Tree-Structured Methods for Longitudinal Data. *Journal of the American Statistical Association*, 87(418):407–418.

Sela, R. J. and Simonoff, J. S. (2011). RE-EM Trees: A New Data Mining Approach for Longitudinal Data. *Machine learning*, 86(2):169–207.

Sigrist, F. (2020). Gaussian Process Boosting. *arXiv preprint arXiv:2004.02653*.

Śmieja, M., Struski, Ł., Tabor, J., Zieliński, B., and Spurek, P. (2018). Processing of missing data by neural networks. *Advances in Neural Information Processing Systems*, 31.

Srivastava, N., Hinton, G., Krizhevsky, A., Sutskever, I., and Salakhutdinov, R. (2014). Dropout: A Simple Way to Prevent Neural Networks from Overfitting. *Journal of Machine Learning Research*, 15(1):1929–1958.

van der Steeg, A., Keyzer-Dekker, C., De Vries, J., and Roukema, J. (2011). Effect of abnormal screening mammogram on quality of life. *Journal of British Surgery*, 98(4):537–542.

Strum, W. B. (2016). Colorectal Adenomas. *New England Journal of Medicine*, 374(11):1065–1075.

Sung, H., Ferlay, J., Siegel, R. L., Laversanne, M., Soerjomataram, I., Jemal, A., and Bray, F. (2021). Global Cancer Statistics 2020: GLOBOCAN Estimates of Incidence and Mortality Worldwide for 36 Cancers in 185 Countries. *CA: A Cancer Journal for Clinicians*, 71(3):209–249.

Tandon, R., Adak, S., and Kaye, J. A. (2006). Neural networks for longitudinal studies in Alzheimer's disease. *Artificial Intelligence in Medicine*, 36(3):245–255.

Thanikachalam, K. and Khan, G. (2019). Colorectal Cancer and Nutrition. *Nutrients*, 11(1):164.

Thrumurthy, S. G., Thrumurthy, S. S., Gilbert, C. E., Ross, P., and Haji, A. (2016). Colorectal adenocarcinoma: risks, prevention and diagnosis. *British Medical Journal*, 354.

Torgo, L., Ribeiro, R. P., Pfahringer, B., and Branco, P. (2013). SMOTE for Regression. In *Portuguese Conference on Artificial Intelligence*, pages 378–389. Springer.

Toribara, N. W. and Sleisenger, M. H. (1995). Screening for Colorectal Cancer. *New England Journal of Medicine*, 332(13):861–867.

Torre, L. A., Bray, F., Siegel, R. L., Ferlay, J., Lortet-Tieulent, J., and Jemal, A. (2015). Global Cancer Statistics, 2012. *CA: A Cancer Journal for Clinicians*, 65(2):87–108.

Tutz, G. and Groll, A. (2010). Generalized Linear Mixed Models Based on Boosting. In *Statistical Modelling and Regression Structures*, pages 197–215. Springer.

Van Buuren, S. (2018). *Flexible Imputation of Missing Data*. CRC press.

Van Buuren, S. and Oudshoorn, K. (1999). *Flexible multivariate imputation by MICE*. TNO Prevention and Health.

van Duuren, L. A., Ozik, J., Spliet, R., Collier, N. T., Lansdorp-Vogelaar, I., and Meester, R. G. (2022). An Evolutionary Algorithm to Personalize Stool-Based Colorectal Cancer Screening. *Frontiers in Physiology*, page 2515.

Wardle, J., Williamson, S., Sutton, S., Biran, A., McCaffery, K., Cuzick, J., and Atkin, W. (2003). Psychological Impact of Colorectal Cancer Screening. *Health Psychology*, 22(1):54.

Welch, H. G. and Black, W. C. (2010). Overdiagnosis in cancer. *Journal of the National Cancer Institute*, 102(9):605–613.

Whitlock, E. P., Lin, J. S., Liles, E., Beil, T. L., and Fu, R. (2012). Screening for Colorectal Cancer: A Targeted, Updated Systematic Review for the U.S. Preventive Services Task Force. *Annals of Internal Medicine*, 157(2):120–134.

Winawer, S. J. (2007). Colorectal cancer screening. *Best Practice & Research Clinical Gastroenterology*, 21(6):1031–1048.

Wu, Y., Xiang, C., Jia, M., and Fang, Y. (2022). Interpretable classifiers for prediction of disability trajectories using a nationwide longitudinal database. *BioMed Central Geriatrics*, 22(1):1–17.

Xiong, Y., Kim, H. J., and Singh, V. (2019). Mixed Effects Neural Networks (MeNets) With Applications to Gaze Estimation. In *Proceedings of the IEEE/CVF Conference on Computer Vision and Pattern Recognition (CVPR)*.

Yang, Y., Qian, W., and Zou, H. (2018). Insurance Premium Prediction via Gradient Tree-Boosted Tweedie Compound Poisson Models. *Journal of Business & Economic Statistics*, 36(3):456–470.

Zorzi, M., Fedeli, U., Schievano, E., Bovo, E., Guzzinati, S., Baracco, S., Fedato, C., Saugo, M., and Dei Tos, A. P. (2015). Impact on colorectal cancer mortality of screening programmes based on the faecal immunochemical test. *Gut*, 64(5):784–790.

Appendices

A Data

The data cleaning procedure is as follows. We first delete variables which are inane to this papers analysis (e.g., information on the morphology and topography of a cancer), and variables which possibly contain patient sensitive information (e.g., participation date, patient pseudonym, and invitation date). We then remove individuals with invalid or missing entries, individuals who returned to the data set after a positive FIT, and individuals younger than 55 or older than 77 in round 1 of 2014. The final data set only includes individuals who participated in two or more consecutive rounds and those who participated in one round at most.

With respect to data engineering, we first transform `result` to attain three categories: favourable, unfavourable, and missing. Here, 'unfavourable' contains all observations with '*unfavourable*' and '*unfavourable (unreliable)*' as result, and 'favourable' contains only observations with '*favourable*' as result. The remaining observations are cast to 'missing', and are deleted from the data set. Hereafter, given that the results of the FIT are based on two thresholds: 275 ng/ml and 47 μg/g, we multiply observations where `haemoglobin current` is based on 275 as threshold by $\frac{47}{275}$, such that all haemoglobin values are represented in the same unit. Finally, we create the following variables: `haemoglobin previous`, `haemoglobin max`, `haemoglobin min`, and we perform one-hot-encoding to `FIT number` and `stage`. More detailed descriptions of each of the variables in the final data set are shown in Table 1.

A.1 MICE

This research employs Multiple Imputation via Chained Equations (MICE) to impute missing values in the stage variable of the original data set. To run this algorithm we create a data set consisting of two data sets from the Dutch screening program and a simulated population run in MISCAN-Colon. Table 6 shows a subset of the combined data. Note that the the '15 threshold' data set contains information on all variables at all times, while the simulated population never contains information on `haemoglobin current` and the original data set only contains information on `stage` 3.8% of the time. Table 7 shows descriptive statistics for each of the additional data sets.

The MICE iterations are as follows:

1 First replace all missing values with placeholders. In this case, all missing values are replaced by a random draw of data (with replacement) within each respective variable.

2.1 Remove the placeholder of `haemoglobin current`.

2.2 Use random sampling to impute all missing values in `haemoglobin current`.

3.1 Remove the placeholder of `stage`.

3.2 Using the newly imputed `haemoglobin current` in combination with `result`, `age` and `sex`, perform predictive mean matching to impute `stage`.

Once these steps are complete, we have completed one full cycle of MICE. We perform 5 × 10 cycles, after which we are left with five distinct imputed `stage` variables. We then compare the distribution of stages in each of these imputed variables to the distribution of stages in the 'MISCAN simulation' data set, and select the imputed variable which most closely matches the distribution in the MISCAN `stage` to replace the original `stage`. Finally, we drop the '15 threshold' and 'MISCAN simulation' data sets.

Table 6: Multiple Imputation via Chained Equations exemplified

Step 0

ID	Result	Age	Sex	Hb	Stage
471	Negative	68	Female	0	NA
471	Negative	70	Female	20.0	NA
471	Positive	72	Female	307.1	4
⋮					
151	Negative	73	Male	37.3	1
152	Positive	73	Female	47.7	2
⋮					
MI1	Negative	65	Male	NA	1
MI1	Negative	58	Male	NA	2

Step 1

ID	Result	Age	Sex	Hb	Stage
471	Negative	68	Female	0	2
471	Negative	70	Female	20.0	2
471	Positive	72	Female	307.1	4
⋮					
151	Negative	73	Male	37.3	1
152	Positive	73	Female	47.7	2
⋮					
MI1	Negative	65	Male	37.3	1
MI1	Negative	58	Male	47.7	2

Step 2.1

ID	Result	Age	Sex	Hb	Stage
471	Negative	68	Female	0	2
471	Negative	70	Female	20.0	2
471	Positive	72	Female	307.1	4
⋮					
151	Negative	73	Male	37.3	1
152	Positive	73	Female	47.7	2
⋮					
MI1	Negative	65	Male	?	1
MI1	Negative	58	Male	?	2

Step 2.2

ID	Result	Age	Sex	Hb	Stage
471	Negative	68	Female	0	2
471	Negative	70	Female	20.0	2
471	Positive	72	Female	307.1	4
⋮					
151	Negative	73	Male	37.3	1
152	Positive	73	Female	47.7	2
⋮					
MI1	Negative	65	Male	20.8	1
MI1	Negative	58	Male	42.6	2

Step 3.1

ID	Result	Age	Sex	Hb	Stage
471	Negative	68	Female	0	?
471	Negative	70	Female	20.0	?
471	Positive	72	Female	307.1	4
⋮					
151	Negative	73	Male	37.3	1
152	Positive	73	Female	47.7	2
⋮					
MI1	Negative	65	Male	20.8	1
MI1	Negative	58	Male	42.6	2

Step 3.2

ID	Result	Age	Sex	Hb	Stage
471	Negative	68	Female	0	1
471	Negative	70	Female	20.0	1
471	Positive	72	Female	307.1	4
⋮					
151	Negative	73	Male	37.3	1
152	Positive	73	Female	47.7	2
⋮					
MI1	Negative	65	Male	20.8	1
MI1	Negative	58	Male	42.6	2

Notes: This table represents an exemplified version of one full cycle of Multiple Imputation via Chained Equations. The data set consists of individuals from the original, the '15 threshold' and the 'MISCAN simulation' data set, denoted by 47*, 15* and MI* as `ID` preface, respectively. The red numbers in Step 1 are obtained from a random draw with replacement from the full data set. The red numbers in Step 2.2 and 3.2 are obtained through predictive mean matching using all variables except the one that will be imputed (i.e., excluding the variable with a question mark in Step 2.1 and 3.1, respectively). `Hb` represents `haemoglobin current`. For more information on each variable see Table 1. The numbers in this table are for illustrative purposes only.

Table 7: Descriptive statistics of additional data sets required for performing MICE

Variable	**Data set**	
	MISCAN simulation	15 threshold
`Age`	$[55; 77]$	$[56; 76]$
`Haemoglobin current`	–	$[0; 292.8]^*$
`Haemoglobin threshold`	–	$[15, 45, 88, 275]$
`Sex`	0 (Male, 48%), 1 (Female, 52%)	0 (Male, 58.2%), 1 (Female, 47.8%)
`Stage`	1 (Healthy, 84.3%), 2 (Non-advanced adenoma, 8.3%), 3 (Advanced adenoma, 7.0%), 4 (Colorectal cancer, 0.4%)	1 (Healthy, 20.4%), 2 (Non-advanced adenoma, 28.9%), 3 (Advanced adenoma, 42.8%), 4 (Colorectal cancer, 7.9%)

Notes: *The '15 threshold' data set contains five observations with `haemoglobin current` below the (lowest) threshold of 15 μg/g, which were not deleted since `stage` was known.

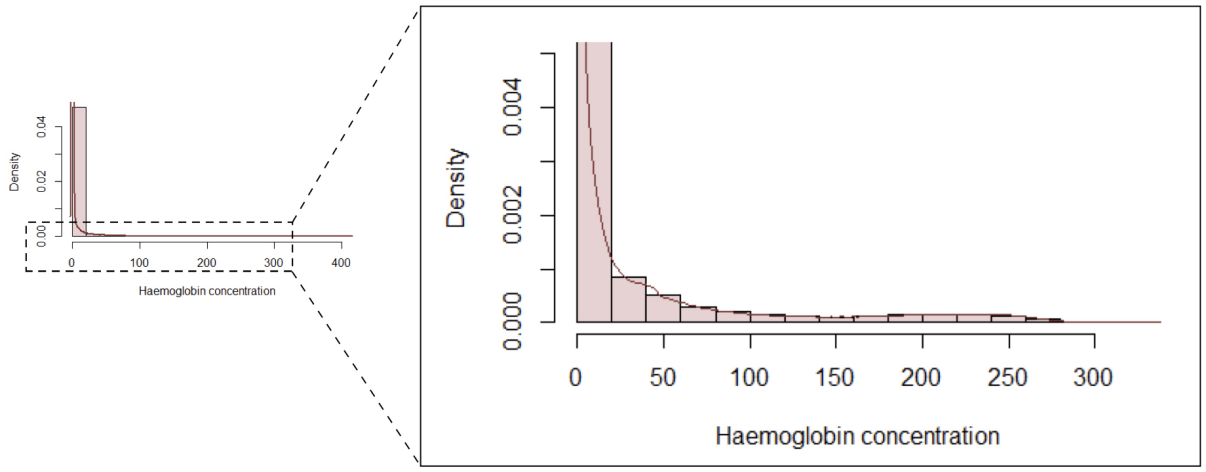

Figure 8: Zoomed in rendition of the distribution of haemoglobin concentrations in Figure 4a

We can see this data can not be fitted to the normal distribution, Poisson can also be discarded because this is not a count data. Another option we can think of Gamma, but this distribution does not take zero values. So, finally, we are left with Tweedie distribution which might be the best fit for this data.

TO DO: nog iets van deze link er in verwerken? https://towardsdatascience.com/insurance-risk-pricing-tweedie-approach-1d71207268fc

B MERT, (G)MERT, RE-EM, and MEml

We have discussed six (of the most) influential papers in the field of machine learning in longitudinal data. The pioneer in this field is Segal (1992), whose goal is to extend tree based methods to clustered data. The approach is quite straightforward; he modifies the split function for each node to accommodate multiple responses. Though this method is a step in the right direction, it has its shortcomings. First, it only allows for equal observations within individuals, which is not always representative (at least not in our case). Second, it does not allow for splits on observation-level covariates, i.e., all observations within a cluster/individual end up in the same terminal node, as they remain together during the tree building process. As a result it is not possible to exploit time-varying values of attributes observed after the first period to predict observations within clusters/individuals[15]. Third, the estimated response value at each node is calculated as a vector of means per node. Thus, this method cannot be used to predict periods ahead, as calculating the mean requires observations for this period.

Acknowledging these shortcomings, many new and improved methods have been proposed including Sela and Simonoff's (2011) random-effects expectation-maximization (RE-EM) trees, Hajjem et al.'s (2011) mixed-effects regression trees (MERT), Hajjem et al.'s (2014) mixed-effects regression forests (MERF), Hajjem et al.'s (2017) generalised mixed-effects regression trees (GMERT), and lastly Ngufor et al.'s (2019) mixed-effects machine learning (MEml) models. In what follows, we provide extensive explanations and mathematical formulations of all five approaches.

B.1 RE-EM trees

Sela and Simonoff (2011) propose their tree-based RE-EM method with a similar goal in mind as Sela and Simonoff (2011): extending tree based algorithms to longitudinal data, but this time through incorporating object-specific random effects. They propose to estimate the fixed- and random-effects using an algorithm reminiscent to Laird and Ware's (1982) expectation-maximisation algorithm.

To explain this method, we first introduce some notation adopted from Hajjem et al. (2017). Define $y_i = [y_{i1}, \ldots, y_{in_i}]^\top$ as the $n_i \times 1$ vector of responses for the n_i observations in cluster $i = 1, \ldots, n$. Let $X_i = [x_{i1}, \ldots, x_{in_i}]^\top$ denote the $n_i \times p$ matrix of fixed-effects covariates, and $Z_i = [z_{i1}, \ldots, z_{in_i}]^\top$ denote the $n_i \times q$ matrix of random-effects covariates. Let b_i denote the $q \times 1$ unknown vector of random effects

[15] Consider for example a node splitting on whether it is the first round or a later round, the latter splits again into second round or higher, and a final split is made for the distinction of the third or fourth round. In this case, we can use the current round value in prediction, exploiting the time-varying values of the covariates. In the Segal (1992) method, however, a single set of attributes is used for all observations within an individual, such that it would not possible to split on, e.g., current round. Hence, it is near impossible to exploit the time-varying information beyond the first period. The only possible way would be to use *all* observations of a time-varying covariate in prediction. However, this most likely will not be useful in practice as including such observations can result in using future information to predict past observations.

for cluster i[16]. The proposed model follows this functional form:

$$\begin{aligned} y_i &= f(X_i) + Z_i b_i + \varepsilon_i \\ b_i &\sim N(0, D), \varepsilon_i \sim N(0, R_i) \\ i &= 1, \ldots, n. \end{aligned} \tag{4}$$

Moreover, any tree-based algorithm recursively partitions the feature space into disjoint regions such that observations with similar response values y_i are grouped together. Adopting (part of) the notation by Ngufor et al. (2019), let $\mathbf{R}_v$ denote the collection of these disjoint regions $v = 1, \ldots, V$. The unknown functional relationship between the response and the predictors can be written as

$$f(x) \equiv \sum_{v=1}^{V} c_v \mathbf{I}(X_i \in \mathbf{R}_v), \tag{5}$$

where c_v is the constant term for the v'th region and second term is the indicator function mapping X_i to regions in $\mathbf{R}_v$.

Using this notation, we present the RE-EM method in Algorithm 1. To estimate the population-level fixed effects, $\hat{f}$, Sela and Simonoff (2011) fit a regression tree (although any tree-based algorithm can be used) using adjusted response variables from which the estimated random effects, $Zi\hat{b}_i$, have been removed. Based on this fitted regression tree, they create a set of terminal nodes, which are then used to fit a linear mixed effects (LME) model to estimate the random effects using (restricted) maximum likelihood. The RE-EM model, in contrast Segal's (1992) model, allows for each node to be split on any covariate, such that different observations for the same object may be placed in different nodes. They also allow for unbalanced panels.

Algorithm 1: RE-EM

Data: Longitudinal or clustered data: $\{(x_{ij}, y_{ij}), i = 1, \ldots, n, j = 1, \ldots, n_i\}$
Result: Estimated machine learning model $\hat{f}$ and random-effects $\hat{b}_i$
Set $r = 0$. Let $\hat{b}_i = 0$;
while *Change in (restricted) likelihood function* $> \epsilon$ **do**
  $r \longleftarrow r + 1$
  E-step:
  (i) $y^*_{i(r)} = y_i - Z_i \hat{b}_{i(r-1)}, i = 1, \ldots, n$;
  (ii) Let $\hat{f}(X_i)_{(r)}$ an estimate of $f(X_i)$ obtained from a standard tree algorithm with $y^*_{i(r)}$ as responses and $X_i, i = 1, \ldots, n$, as covariates;
  (iii) Use this regression tree to create a set of indicator variables, $\mathbf{I}(X_i \in \mathbf{R}_v)_{(r)}$, where v ranges over all of the terminal nodes in the tree;

  M-step:
  (i) Fit the linear mixed effects model, $y_i = Z_i b_i + \mathbf{I}(X_i \in \mathbf{R}_v) c_v + \varepsilon_{it}$. Extract $\hat{b}_{i(r)}$ from the estimated model.
end

[16]Clearly, this notation can be easily extended to longitudinal data, if we define each individual as it's own group, such $j = 1, \ldots, n_i$ represent the observations for each individual $i = 1, \ldots, n$.

B.2 MERT

Hajjem et al. (2011) propose another method for longitudinal data using tree-based methods. Their MERT model aims to dissociate the fixed effects from random effects, and follows the same functional form as presented in Equation 4. Similar to Sela and Simonoff (2011), MERT also allows for modeling unbalanced clusters and splitting on observation-level covariates. Moreover, MERF also estimates the fixed- and random effects in an expectation-maximization manner. Specifically, Algorithm 2 shows that MERT uses a standard regression tree to model the fixed-effects, and a LME with (restricted) maximum likelihood to estimate the random-effects. This process repeats itself until the generalised log-likelihood (GLL) is smaller than a predetermined tolerance value ϵ.

We distinguish two (main) differences between MERT and RE-EM trees. First, MERT assumes that all correlation is induced solely via between-subject variation, – i.e., R_i is assumed to be diagonal – whereas RE-EM allows for more general correlation structures, such that R_i is allowed to be non-diagonal. Second, the modeling of random-effects in MERT is node-invariant, whereas RE-EM trees obviously are not.

Algorithm 2: MERT

Data: Longitudinal or clustered data: $\{(x_{ij}, y_{ij}), i = 1, \ldots, n, j = 1, \ldots, n_i\}$
Result: Estimated machine learning model $\hat{f}$ and random-effects $\hat{b}_i$
Set $r = 0$. Let $\hat{b}_{i(0)} = 0, \hat{\sigma}^2_{(0)} = 1$, and $\hat{D}_{(0)} = I_q$.
while *Change in GLL* $> \varepsilon$ **do**
$r \longleftarrow r + 1$
E-step:
(i) $y^*_{i(r)} = y_i - Z_i \hat{b}_{i(r-1)}, i = 1, \ldots, n$;
(ii) Let $\hat{f}(X_i)_{(r)}$ an estimate of $f(X_i)$ obtained from a standard tree algorithm with $y^*_{i(r)}$ as responses and $X_i, i = 1, \ldots, n$, as covariates;
(iii) $\hat{b}_{i(r)} = \hat{D}_{(r-1)} Z_i^T \hat{V}^{-1}_{i(r-1)} \left(y_i - \hat{f}(X_i)_{(r)}\right), i = 1, \ldots, n$, where $\hat{V}_{i(r-1)} = Z_i \hat{D}_{(r-1)} Z_i^T + \hat{\sigma}^2_{(r-1)} I_{n_i}, i = 1, \ldots, n$;

M-step:
(i) $\hat{\sigma}^2_{(r)} = N^{-1} \sum_{i=1}^n \left\{ \hat{\varepsilon}^T_{i(r)} \hat{\varepsilon}_{i(r)} + \hat{\sigma}^2_{(r-1)} \left[n_i - \hat{\sigma}^2_{(r-1)} \text{trace}\left(\hat{V}_{i(r-1)}\right) \right] \right\}$, where $\hat{\varepsilon}_{i(r)} = y_i - \hat{f}(X_i)_{(r)} - Z_i \hat{b}_{i(r)}$;
(ii) $\hat{D}_{(r)} = n^{-1} \sum_{i=1}^n \left\{ \hat{b}_{i(r)} \hat{b}^T_{i(r)} + \left[\hat{D}_{(r-1)} - \hat{D}_{(r-1)} Z_i^T \hat{V}^{-1}_{i(r-1)} Z_i \hat{D}_{(r-1)} \right] \right\}$.
end

B.3 MERF

Further improvement of the predictive accuracy of MERT could be achieved when used as the base learner in an ensemble algorithms. Consequently, Hajjem et al. (2014) introduce MERF, which generalizes MERT through replacing the regression trees within each iteration in MERT with a forest of regression trees. MERF follows the same functional form as MERT and RE-EM (see Equation 4) and also assumes R_i is diagonal.

The approach is detailed in Algorithm 3. Each step in MERF which is identical to that in MERT is presented in gray, to highlight the similarities between both methods. Clearly, they only differ in step

two of the expectation-step in which the regression forest is built. Besides the premise of the algorithm and most of the algorithm itself being similar in MERT and MERF, the difference in step two comes with an additional assumption. One must resample observations in order to build random forests, which is done through bootstrapping in this case. For optimal performance of bootstrapping, it is required that the observations are i.i.d.. Consequently, we must assume that the random effects $Z_i b_i$ fully explain the correlation within clusters/individuals, such that y_i^* is i.i.d. once the random effects have been removed.

Algorithm 3: MERF

Data: Longitudinal or clustered data: $\{(x_{ij}, y_{ij}), i = 1, \ldots, n, j = 1, \ldots, n_i\}$

Result: Estimated machine learning model $\hat{f}$ and random-effects $\hat{b}_i$

Set $r = 0$. Let $\hat{b}_{i(0)} = 0, \hat{\sigma}^2_{(0)} = 1$, and $\hat{D}_{(0)} = I_q$.;

while *Change in GLL* $> \varepsilon$ **do**

$r \longleftarrow r + 1$

E-step:

(i) $y^*_{i(r)} = y_i - Z_i \hat{b}_{i(r-1)}, i = 1, \ldots, n$;

(ii.a) Build a forest of trees using a standard RF algorithm with $y^*_{ij(r)}$ as the training set responses and x_{ij} as the corresponding training set of covariates, $i = 1, ..., n, j = 1, ..., n_i$. The bootstrap training samples to build the forest are simple random samples drawn with replacement from the training set $y^*_{ij(r)}, x_{ij}$;

(ii.b) Estimate $\hat{f}(x_{ij})_{(r)}$ using only the subset of trees in the forest that are built with the bootstrap samples not containing y^*_{ij}, that is, the out-of-bag prediction of the RF;

(ii.c) Let $\hat{f}(X_i)_{(r)} = \left[\hat{f}(x_{i1})_{(r)}, ..., \hat{f}(x_{in_i})_{(r)}\right]$;

(iii) $\hat{b}_{i(r)} = \hat{D}_{(r-1)} Z_i^T \hat{V}^{-1}_{i(r-1)} \left(y_i - \hat{f}\left(X_i\right)_{(r)}\right), i = 1, \ldots, n$, where

$\hat{V}_{i(r-1)} = Z_i \hat{D}_{(r-1)} Z_i^T + \hat{\sigma}^2_{(r-1)} I_{n_i}, i = 1, \ldots, n$;

M-step:

(i) $\hat{\sigma}^2_{(r)} = N^{-1} \sum_{i=1}^n \left\{\hat{\varepsilon}^T_{i(r)} \hat{\varepsilon}_{i(r)} + \hat{\sigma}^2_{(r-1)} \left[n_i - \hat{\sigma}^2_{(r-1)} \text{trace}\left(\hat{V}_{i(r-1)}\right)\right]\right\}$, where

$\hat{\varepsilon}_{i(r)} = y_i - \hat{f}\left(X_i\right)_{(r)} - Z_i \hat{b}_{i(r)}$;

(ii) $\hat{D}_{(r)} = n^{-1} \sum_{i=1}^n \left\{\hat{b}_{i(r)} \hat{b}^T_{i(r)} + \left[\hat{D}_{(r-1)} - \hat{D}_{(r-1)} Z_i^T \hat{V}^{-1}_{i(r-1)} Z_i \hat{D}_{(r-1)}\right]\right\}$.;

end

B.4 GMERT and MEml

RE-EM, MERT and MERF are all designed for Gaussian response data. In practice, it can be useful to also model non-Gaussian (e.g., binary) response data. To this end, we introduce the GMERT model by Hajjem et al. (2017) and the MEml model by Ngufor et al. (2019). Both approaches are based on GLMM, and allow for non-Gaussian dependent variables.

Adopting the notation by Hajjem et al. (2017) the GLMM assumes that the response vector y_i, conditional on the (assumed i.i.d. normal) random effects b_i, is independent and follows a distribution from the exponential family with density

$$f\left(y_i \mid b_i, \beta\right),$$

where the fixed-effects parameter $\beta_{[p\times 1]}$ is an unknown common vector over all clusters. Now, define

$$\eta_i = g(\mu_i) = g\left(E\left(y_i \mid b_i\right)\right),$$
$$\operatorname{Cov}\left(y_i \mid b_i\right) = \sigma^2 v_i\left(\mu_i\right),$$

where $\eta_i = g\left(\mu_i\right)_{[n_i\times 1]}$ denotes the population fixed-effect parameters with known link function $g(\cdot)$, possibly known σ^2 a dispersion parameter, and known variance function $v(\cdot)$ where $v_i\left(\mu_i\right)$ a $n \times n_i$ diagonal matrix with $v(\mu_{ij})$ as elements. The GLMM assumes a parametric distribution and imposes restrictive linear relationships between the link function and the covariates.

The proposed GMERT and MEml models can be written as

$$\begin{aligned} \eta_i &= f\left(X_i\right) + Z_i b_i, \\ b_i &\sim N(0, D), \\ i &= 1, \ldots, n. \end{aligned} \tag{6}$$

Then, following the PQL approach, the data is approximated by $\tilde{y}_i = \mu_i + e_i$ and then taking the first order Taylor expansion about the current parameter estimates, which results in

$$\tilde{y}_i = g\left(\hat{\mu}_i\right) + \left(y_i - \hat{\mu}_i\right) g'\left(\hat{\mu}_i\right), \tag{7}$$

which can be simultaneously defined as

$$\tilde{y}_i = f\left(X_i\right) + Z_i b_i + e_i. \tag{8}$$

B.4.1 GMERT

Hajjem et al. (2017)'s GMERT model extends their aforementioned MERT model through replacing the linear structure normally used to model fixed-effect component in GLMMs with a regression tree structure. The estimation of the random component is still represented using a linear structure, as in GLMMs. Algorithm 3 presents the GMERT pseudocode, again with gray parts indicating identical steps to Hajjem et al.'s (Hajjem et al. (2011)) MERT model (see Algorithm 2).

The aim of the transformation of $\tilde{y}_i$ in Equation 7 is to make the outcome behave like a normally distributed variable, for which a LME model can be fitted. Or, in the GMERT case, to fit the MERT approach, which is designed for a normally distributed outcome. Clearly, the inner while loop in Algorithm 4 almost perfectly coincides with the MERT algorithm apart from a weight factor (shown in red) and the definition of the responses (although any tree-based algorithm could be used). Once the inner loop has been completed, each of the variables in the weighted LME pseudo-model are updated until convergence of the estimated population fixed-effect parameter $\hat{\eta}_i$. Algorithm 4 also clearly shows one drawback of GMERT. That is, GMERT is computationally expensive as the algorithm is a doubly iterating process, which requires many trees to be built (Hajjem et al., 2017).

Algorithm 4: GMERT

Data: Longitudinal or clustered data: $\{(x_{ij}, y_{ij}), i = 1, \ldots, n, j = 1, \ldots, n_i\}$

Result: Estimated machine learning model $\hat{f}$ and random-effects $\hat{b}_i$

Set $M = 0$, $m = 0$. Given initial estimates of the mean values, $\hat{\mu}_{ij}^{(0)}, j = 1, \ldots, n_i$, fit a weighted LME pseudo-model using the linearised pseudo responses, $\tilde{y}_i^{(0)} = g\left(\hat{\mu}_i^{(0)}\right) + \left(y_i - \hat{\mu}_i^{(0)}\right) g'\left(\hat{\mu}_i^{(0)}\right)$, and the weights, $W_i^{(0)} = \text{diag}\left(w_{ij}^{(0)}\right)$ where $w_{ij}^{(0)} = \left(v_{ij} g'\left(\hat{\mu}_{ij}^{(0)}\right)^2\right)^{-1}$. Let $\hat{\sigma}^2_{(0)}$ and $\hat{D}_{(0)}$ be the estimates of this weighted LME pseudo-model. **while** *non-convergence of* $\hat{\eta}_i$ **do**

$M \longleftarrow M + 1$

while *Change in GLL* $> \epsilon$ **do**

Denote $\tilde{y}_{i(m)} := y_{i(m)}$; // Only to illustrate similarity between MERT

$m \longleftarrow m + 1$

E-step:

(i) $y^*_{i(m)} = y_i^{(M)} - Z_i \hat{b}_{i(m-1)}$;

(ii) Let $\hat{f}\left(X_i\right)_{(m)}$ be an estimate of $f\left(X_i\right)$ obtained from a standard regression tree algorithm with $y^*_{i(m)}$ as responses, X_i as covariates, and W_i as weights, $i = 1, \ldots, n$;

(iii) $\hat{b}_{i(m)} = \hat{D}_{(m-1)} \left(W_i^{\frac{1}{2}(M)} Z_i\right)^T \hat{V}^{-1}_{i(m-1)} \left(W_i^{\frac{1}{2}(M)} y_i^{(M)} - W_i^{\frac{1}{2}(M)} \hat{f}_{(m)}\left(X_i\right)\right)$, where

$\hat{V}_{i(m-1)} = W_i^{\frac{1}{2}(M)} Z_i \hat{D}_{(m-1)} \left(W_i^{\frac{1}{2}(M)} Z_i\right)^T + \hat{\sigma}^2_{(m-1)} I_{n_i}, i = 1, \ldots, n.$;

M-step:

(i) $\hat{\sigma}^2_{(m)} = N^{-1} \sum_{i=1}^{n} \left\{\hat{\varepsilon}^T_{i(m)} \hat{\varepsilon}_{i(m)} + \hat{\sigma}^2_{(m-1)} \left[n_i - \hat{\sigma}^2_{(m-1)} \text{trace}\left(\hat{V}_{i(m-1)}\right)\right]\right\}$, where

$\hat{\varepsilon}_{i(m)} = W_i^{\frac{1}{2}(M)} y_i^{(M)} - W_i^{\frac{1}{2}(M)} \hat{f}_{(m)}\left(X_i\right) - W_i^{\frac{1}{2}(M)} Z_i \hat{b}_{i(m)}$;

(ii) $\hat{D}_{(m)} = n^{-1} \sum_{i=1}^{n} \left\{\hat{b}_{i(m)} \hat{b}^T_{i(m)} + \left[\hat{D}_{(m-1)} - \hat{D}_{(m-1)} \left(W_i^{\frac{1}{2}(M)} Z_i\right)^T \hat{V}^{-1}_{i(m-1)} W_i^{\frac{1}{2}(M)} Z_i \hat{D}_{(m-1)}\right]\right\}$;

end

(i) $\hat{\eta}_i^{(M)} = \hat{f}_{(m)}\left(X_i\right) + Z_i \hat{b}_{i(m)}$;

(ii) $\hat{\mu}_i^{(M)} = g^{-1}\left(\hat{\eta}_i^{(M)}\right)$;

(iii) $\tilde{y}_i^{(M)} = g\left(\hat{\mu}_i^{(M)}\right) + \left(\tilde{y}_i - \hat{\mu}_i^{(M)}\right) g'\left(\hat{\mu}_i^{(M)}\right)$;

(iv) $w_{ij}^{(M)} = \left(v_{ij} g'\left(\hat{\mu}_{ij}^{(M)}\right)^2\right)^{-1}$;

(v) $W_i^{(M)} = \text{diag}\left(w_{ij}^{(M)}\right)$.

end

B.4.2 MEml

The MEml approach by Ngufor et al. (2019) uses a node-based expectation-maximization approach reminiscent to RE-EM, in a general GLMM framework similar to GMERT. The random effects in Equation 6 and the population-level effects in Equation 8 are alternatively estimated, as shown in Algorithm 5.

First, the random effects are initiated at zero, and are then used to compute the adjusted response variable. Subsequently, a machine learning model is trained to estimate $\hat{f}(X_i)$ from Equation 8 using the adjusted response variables. Depending on the employed machine learning algorithm, the algorithm either extracts rules or terminal nodes for all disjoint regions v. Finally, the random effects are estimated using $\hat{f}(X_i)$ in the functional form shown in Equation 5. This process repeats until convergence.

Algorithm 5: MEml

Data: Longitudinal or clustered data: $\{(x_{ij}, y_{ij}), i = 1, \ldots, n, j = 1, \ldots, n_i\}$

Result: Estimated machine learning model $\hat{f}$ and random-effects $\hat{b}_i$

Set $r = 0$. Let $\hat{b}_{i(0)} = 0$ and $\hat{\mu}_{i(0)} = 0.5$. **while** *Change in GLL* $> \varepsilon$ **do**

$r \longleftarrow r + 1$

E-step:

(i) Compute $\tilde{y}^*_{i(r)} = \left(y_i - \hat{\mu}_{i(r)}\right) g'\left(\hat{\mu}_{i(r)}\right) + g\left(\hat{\mu}_{i(r)}\right)$;

(ii) Let $\hat{f}\left(X_i\right)_{(m)}$ be an estimate of $f\left(X_i\right)$ obtained from a standard RT, GBM, MOB or Ctree algorithm with $\tilde{y}^*_{i(r)} - \hat{\mathbf{b}}_i^\top \mathbf{z}_i$ as responses, X_i as covariates and weights $w_{ij(r)} = \left(v_{ij} g'\left(\hat{\mu}_{ij(r)}\right)^2\right)^{-1}$ for each observation;

if *MOB or Ctree* **then**

(iii) Create a set of indicator variables, $\mathbf{I}\left(X_i \in \mathbf{R}_v\right)_{(r)}$, where v ranges over all of the terminal nodes in the fitted tree object;

else if *RF or GBM* **then**

(iii) Create a set of indicator variables, $\mathbf{I}\left(X_i \in \mathbf{R}_v\right)_{(r)}$, where v is a rule set using inTrees;

end

M-step:

(i) Fit the GLMM model for $\eta_i = \sum_{v=1}^{V} \mathbf{I}\left(\mathbf{X}_i \in \mathbf{R}_v\right) c_v + \mathbf{b}_i^\top \mathbf{z}_i$ and extract estimates of the mixed effects $\hat{b}_{i(r)}$ and mean $\hat{\mu}_{i(r)}$.

end

B.5 Prediction

In the previous sections we have shown the similarities and differences between each model. We now briefly discuss one aspect which is (virtually) the same across each of the aforementioned models: prediction.

We distinguish the prediction of two cases:

1. Predicting observations for new clusters/individuals, with no past observations;
2. Predicting future observations for clusters/individuals within the sample.

TO DO: Scenario twee In the first scenario, the random effects of a cluster is not known. Therefore, each method fixes the estimated random-effects at zero, and only uses the estimated fixed-effects for the prediction. In the second scenario, both the estimated fixed-effects and the estimated random part corresponding to its cluster are used in prediction using the new covariates.

B.6 Method comparison

B.6.1 Performance

Mangino and Finch (2021) find that MEgbm (the GBM version of Ngufor et al.'s (2019) MEml model), MERF, and RE-EM attain similar performance to each other, although (Capitaine et al., 2021; Kilham et al., 2018) find that MERF outperforms RE-EM and GLMM in terms of R^2, RMSE and estimated bias. Moreover, Hajjem et al. (2014) finds that MERF outperforms MERT. Since GMERT is a rather new methodology, there exists little comparative research on this method compared to methods such as RE-EM, MERT and MERF. The same holds for the comparison of MEml to (G)MERT. Therefore, it is difficult to assess the relative performance of these methods.

B.6.2 Mathematical properties

Moreover, even though Hajjem et al. (2011, 2017); Sela and Simonoff (2011) and Ngufor et al. (2019) find that their respective mixed-effects models are always better to use than their single-level counterparts (in presence of random effects), an important point of discussion is convergence of these methods. RE-EM, (G)MERT, MERF, and MEml are each based on the premise of expectation-maximization, and Sela and Simonoff (2011) rightfully note that since these methods are not true EM algorithms, the usual properties of the EM algorithm do not necessarily apply. Although a relatively sizeable body of literature exists on the consistency of regression forests/trees and mixed-effects models; unfortunately, there is only little guidance on the consistency of the methods mentioned here in current literature. For example, Capitaine et al. (2021) investigates the consistency properties of MERF, and find that the fitted MERF forest estimations for the response variable and out-of-sample predictions converge when the number of individuals is large enough ($n \to \infty$). However, the convergence of MERF as a whole, since it is based on an iterative EM-algorithm, requires that the inner RF model must be stabilized. This stabilization only occurs for large values of the number of variables randomly drawn before optimizing the split of a node of a tree in the RF, although it remains unclear what "large" entails. It is also unclear how the convergence properties of MERF hold up in case other machine learning methods are used to estimate the fixed-effects component. Moreover, Hajjem et al. (2017) note that convergence of their algorithm might be dependent on, e.g., the structures and magnitudes of fixed- and random effects, but their research lacks concrete inference on consistency of the estimates. Thus, since assessing the mathematical properties of each method goes beyond the scope of this research, we must join Sela and Simonoff (2011) in their suggestion that further research should be conducted on the consistency of $\hat{f}$ and the estimated random effects.

B.6.3 Model compatibility

A clear disadvantage of RE-EM and (G)MERT, is that these models only allow for tree-based machine learning methods to be used in the estimation of the fixed-effects. MEml allows for the use of any machine learning method, but Ngufor et al. (2019) do not supply any complementary code if one would want to employ any method other than RF, GBM, MOB, or Ctree. In contrast, Hajjem et al. (2014) recently published an updated version of the MERF source-code which has been adjusted in Python to include all types of Python's Sklearn machine learning methods.

In conclusion, based on the (limited) literature on the relative performance of all methods, and compatibility with both tree-based (XGBoost) and non-tree-based (ANNs) machine learning methods, we choose to employ MERF in this analysis.

C Bayesian Hyperopt

Table 8: Tuning parameters for XGBoost

Hyperparameter	Search space	Description
`learning_rate`	$[\log(0.001); \log(1)]$ (log uniform)	Step size shrinkage used in update to prevent overfitting. After each boosting step, we can directly obtain the weights of new features, and the learning rate shrinks the feature weights to make the boosting process more conservative.
`max_depth`	$[2, 6]$ (1)	Maximum depth of a tree. Increasing this value will make the model more complex and more likely to overfit. Beware that the XGBoost algorithm aggressively consumes memory when training a deep tree.
`colsample_bytree`	$[0.5, 1.0]$ (uniform)	The subsample ratio of columns when constructing each tree. Subsampling occurs once for every tree constructed.
`reg_lambda`	$[0.0, 1.0]$ (uniform)	L2 regularization term on weights. Increasing this value will make the model more conservative.
`subsample`	$[0.5, 1.0]$ (uniform)	Subsample ratio of the training instances. Setting it to 0.5 means that the XGBoost algorithm would randomly sample half of the training data prior to growing trees, which will prevent overfitting. Subsampling will occur once in every boosting iteration.
`n_estimators`	$[50, 200]$ (10)	The number of gradient boosted trees. Equivalent to number of boosting rounds. A higher number of estimators usually learns better, which might cause overfitting in turn.
`normalization`[1]	[none, minmax, standardization, quantile]	Data normalisation technique, only applied to train data. Minmax transforms the minimum (maximum) value of each regressor to 0 (1) and interpolates remaining values. Standardization removes the mean and scales to unit variance for each feature. The robust quantile normalization transforms the features to follow a uniform or a normal distribution (also robust).

Notes: This table shows which hyperparameters in the XGBoost model are tuned using Hyperopt, along with their descriptions. The search space is represented within brackets, with the step size in parentheses.
[1]Normalization is technically not a hyperparameter, but it is included in this overview for completeness.

Table 9: Tuning parameters for ANN

Hyperparameter	Search space	Description
`learning_rate`	$[\log(0.001), \log(1)]$ (log uniform)	Step size shrinkage used in update to prevent overfitting. After each boosting step, we can directly obtain the weights of new features, and the learning rate shrinks the feature weights to make the boosting process more conservative.
`batch_size`	$[11, 15]$ (uniform)	The number of samples that will be propagated through the network, calculated as 2^b with b the hyperparameter value. Introducing this parameter is necessary to reduce memory usage and speed up training time, with as disadvantage that the estimate of the gradient might be less accurate.
`n_layers`	$[1, 2]$	Number of hidden layers in the network.
`init_dropout`	$[0.0, 1.0]$ (uniform)	Dropout rate in first hidden layer, where dropout implies temporarily removing a node from the network, along with all its incoming and outgoing connections (Srivastava et al., 2014).
`mid_dropout`	$[0.0, 1.0]$ (uniform)	Dropout rate in the second hidden layer, if present.
`activation`	[ReLu, sigmoid, identity]	Activation function used to progress from layer to layer. The sigmoid and ReLu activation function introduce non-linearity to the neural network.
`n_neurons`	$[8, 240]$ (4)	Total number of neurons used in (both) hidden layer(s).
`normalization`[1]	[none, minmax, standardization, quantile]	Data normalisation technique, only applied to train data. Minmax transforms the minimum (maximum) value of each regressor to 0 (1) and interpolates remaining values. Standardization removes the mean and scales to unit variance for each feature. The robust quantile normalization transforms the features to follow a uniform or a normal distribution (also robust).

Notes: This table shows which hyperparameters in the ANN model are tuned using Hyperopt, along with their descriptions. The search space is represented within brackets, with the step size in parentheses. [1]Normalization is technically not a hyperparameter, but it is included in this overview for completeness.

D Results

D.1 Extra test set

Figure 9: (Predicted) haemoglobin concentration histograms

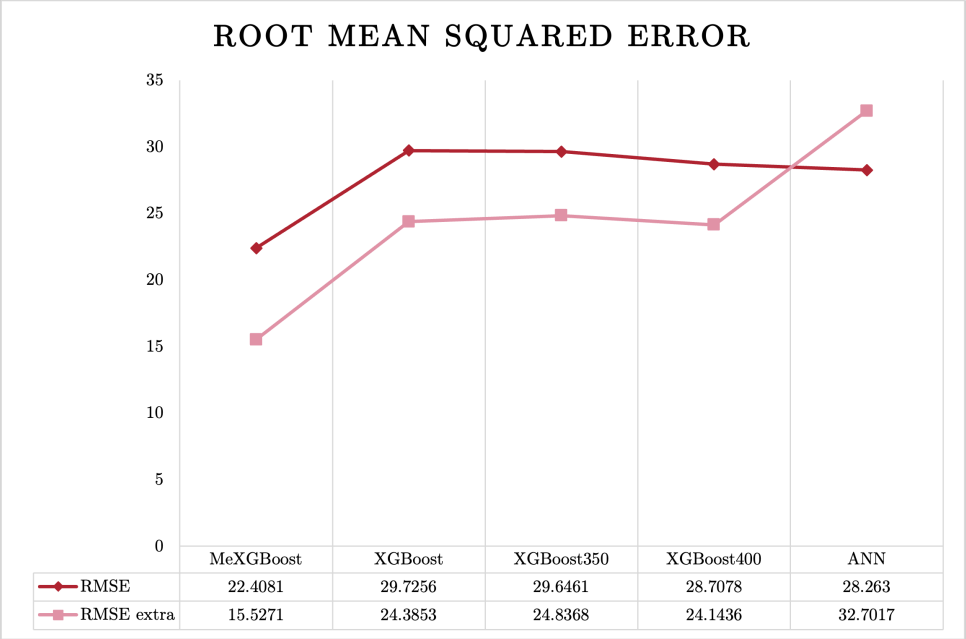

(a) RMSE

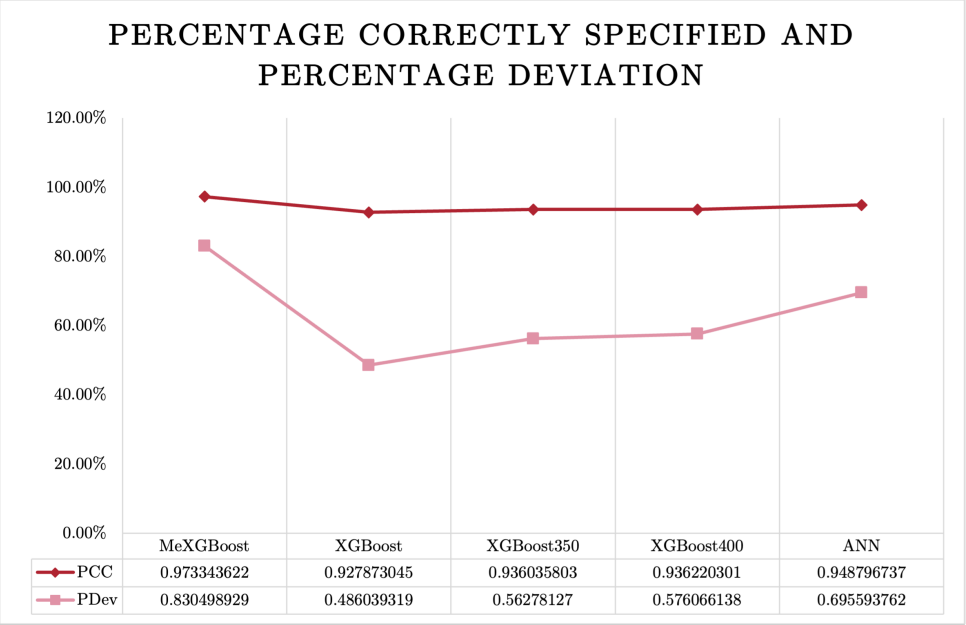

(b) PCC and PDev

TO DO: This is a bit weird, PCC and PDev should also be split up between normal and extra test set, now it's just confusing why subfigure b would be in this part of the appendix.